10

Adaptive Multicarrier CDMA Space-Time Receivers

Besma Smida
Harvard University

Sofiène Affes
University of Quebec

10.1 Motivation of the Chapter

One important challenge for future wireless networks is the design of appropriate transceivers that can reliably transmit high data rates at a high bandwidth efficiency. Multicarrier code division multiple access (MC-CDMA) systems in particular have received considerable attention, because they have the attractive feature of high spectral efficiency and because they can be easily implemented using fast Fourier transform (FFT) without significantly increasing the transmitter and receiver complexities [1, 2].

The multicarrier systems include different combinations of multicarrier modulation (accomplished by orthogonal frequency division multiplex [OFDM]) and direct-sequence code division multiple access (DS-CDMA). This combination provides both high-data-rate transmission and multiple access capabilities. An excellent overview of the different multicarrier CDMA systems is found in [2] and [3]. They can be divided into two categories of multicarrier CDMA: one combines multicarrier modulation with frequency-domain spreading, and the other transmits several DS-CDMA waveforms in parallel with the spreading operation performed in time. The transmitter proposed here belongs to the second group, and it can be divided into MC-DS-CDMA and multitone (MT) CDMA, the difference between the two being the subcarrier frequency separation.

However promising, challenges remain before multicarrier CDMA can achieve its full potential. One open area is the design of transceivers that will enable the future upgrade of current wireless networks beyond the third generation (3G). Transceivers selected for early implementation need to achieve high spectrum efficiency in realistic propagation channels while being robust to imperfections such as time and frequency mismatch. Multicarrier CDMA, similar to other multicarrier schemes, is sensitive to the signal distortion generated by the imperfect frequency downconversion at the receiver due to local oscillator frequency offset. It has been found that carrier frequency offset (CFO) gives rise to a reduction of the useful signal power and to the intercarrier interference (ICI) [5]. Furthermore, one of the major obstacles in detecting multicarrier CDMA signals is interference. The multiple access interference (MAI) and the intersymbol interference (ISI), which are inherited from conventional DS-CDMA, affect likewise the performance of multicarrier CDMA systems.

The subject of this work is the design of a new adaptive multicarrier CDMA space-time receiver that provides solutions to these problems, with particular emphasis on the comparison of the MC-DS-CDMA– and MT-CDMA–air interface configurations. The proposed receiver, named MC-ISR* (multicarrier interference subspace rejection), will hence (1) perform blind channel identification and equalization as well as fast and accurate joint synchronization in time and frequency, and (2) mitigate the full interference effect. In addition, the assessment of this new receiver is oriented toward an implementation in a future, real-world wireless system.

* This work was presented in part at the IEEE SPAWC 2005 and IEEE ISSPA 2005 conferences and accepted for publication in *IEEE Transactions on Vehicular Technology* [6].

10.2 Overview of Multicarrier CDMA for Wireless Communications

In this section, we review concisely the class of multicarrier CDMA schemes, which have been discussed in the literature. Specifically, we discuss their parameters, spectral characteristics, advantages, and disadvantages in terms of design and structure. For more detailed information on the different multicarrier CDMA schemes, the reader is referred to the excellent monographs by Hanzo et al. [3].

The multicarrier CDMA schemes are categorized mainly in two groups. One spreads the original data stream using a given spreading code, and then modulates a different subcarrier with each chip (i.e., the spreading is in the frequency domain), and the other spreads the serial-to-parallel (S/P) converted data streams using a given spreading code, and then modulates a different subcarrier with each of the data streams (spreading is in the time domain).

10.2.1 Frequency-Domain Spreading Multicarrier CDMA: FD-MC-CDMA

Figure 10.1a shows the spectrum of the multicarrier CDMA scheme associated with frequency-domain spreading [7–10]. We refer to this scheme as FD-MC-CDMA. The FD-MC-CDMA transmitter spreads the original data stream over N_c subcarriers using a given spreading code in the frequency domain. This scheme does not include serial-to-parallel data conversion, and there exists no spreading modulation on each subcarrier. Therefore, the data rate on each of the N_c subcarriers is the same as the input data rate. However, by spreading each data bit across all of the N_c subcarriers, the fading effects of multipath channels are mitigated. In this FD-MC-CDMA system, the subcarrier frequencies are chosen to be orthogonal to each other, i.e., the subcarrier frequencies satisfy the following condition:

$$f_i - f_j = \frac{n|i-j|}{T},$$

where $n \in \mathbb{N}$ and T is the symbol duration. Therefore, the minimum spacing Δ between two adjacent subcarriers satisfies $1/T$, which is a widely used assumption [7–10] and is also the case employed in Figure 10.1a. If no overlap is assumed, then the minimum spacing Δ between two adjacent subcarriers is $2/T$.

Yee et al. [7] have considered an FD-MC-CDMA system, in which the subcarriers' frequency separation is higher than the coherence bandwidth of the channel, and therefore the individual subcarriers experience independent fading. As a result, the frequency diversity is maximized. This is the main advantage of the FD-MC-CDMA scheme over other multicarrier CDMA schemes [2]. However, this system may require a considerable transmission bandwidth. Besides that, a large delay spread per subcarrier would lessen this bandwidth requirement. But in a frequency-selective fading channel, different

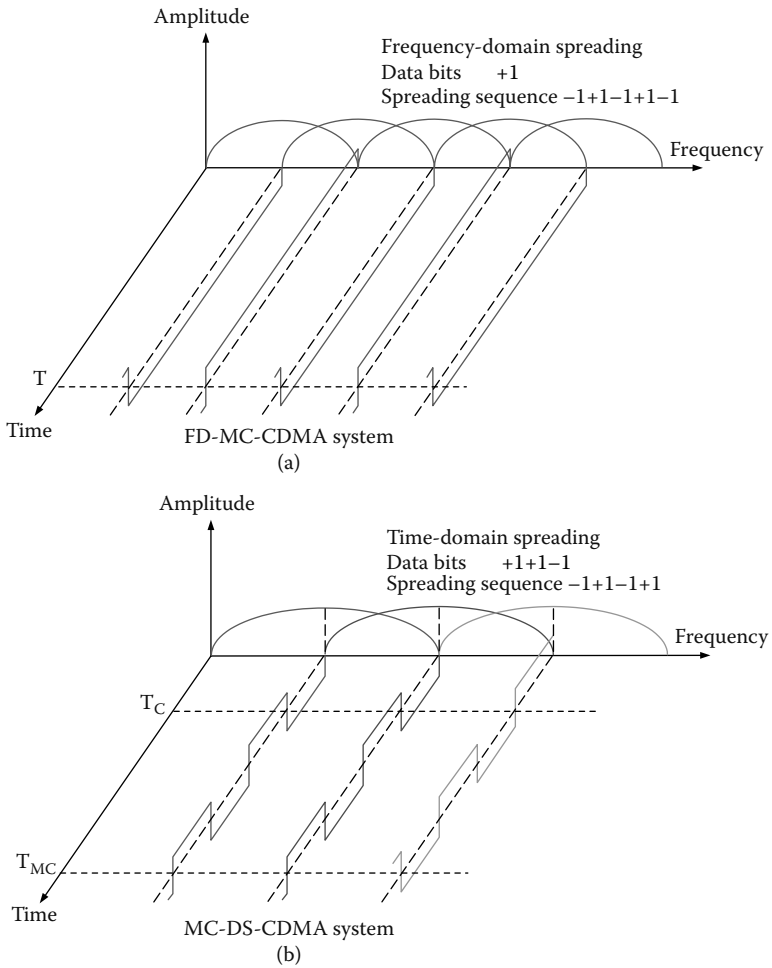

FIGURE 10.1 Spectra of different multicarrier CDMA schemes: (a) FD-MC-CDMA, (b) MC-DS-CDMA, (c) MT-CDMA.

subcarriers may encounter different amplitude attenuations and phase shifts, which can consequently destroy the orthogonality of the subcarriers.

10.2.2 Time-Domain Spreading Multicarrier CDMA: MC-DS-CDMA

In [11], a multicarrier DS-CDMA system named MC-DS-CDMA has been proposed. The MC-DS-CDMA transmitter spreads the serial-to-parallel converted data streams using a given spreading code in the time domain so that the resulting spectrum of each subcarrier can satisfy the orthogonality condition with the minimum frequency separation [11]. This scheme was originally proposed for an uplink communication system, because

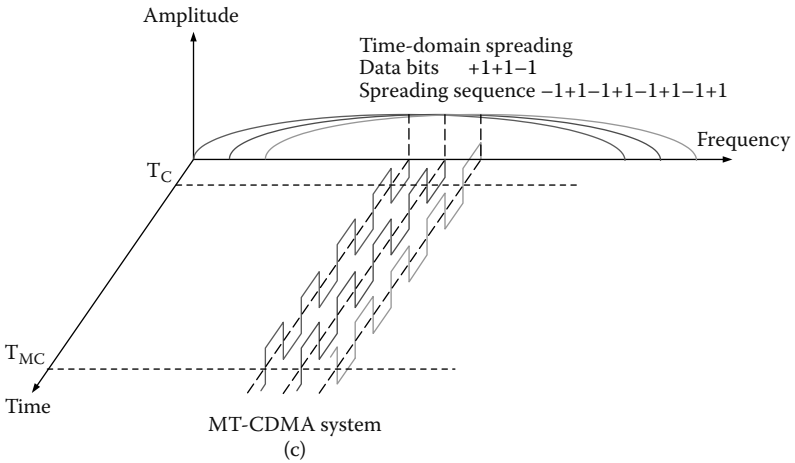

FIGURE 10.1 (continued).

this characteristic is effective for establishing a quasi-synchronous channel. In [12], Kondo and Milstein proposed a similar transmitter, except that band-limited subcarrier signals and larger subcarrier separation are employed. This scheme yields both frequency diversity improvement and narrowband interference suppression. The spectrum of the MC-DS-CDMA signal with 50% overlap having three subcarriers is shown in Figure 10.1b. In the MC-DS-CDMA system, the subcarrier frequencies are usually chosen to be orthogonal to each other after spreading, which can be formulated as

$$f_i - f_j = \frac{n|i-j|}{T_c},$$

where $n \in \mathbb{N}$ and T_c is the chip duration. Therefore, the minimum spacing Δ between two adjacent subcarriers satisfies $1/T_c$.

Frequency diversity in MC-DS-CDMA systems can be achieved by repeating the transmitted signal in the frequency (F) domain with the aid of several subcarriers [12–14]. Alternatively, in MC-DS-CDMA systems the F-domain repetition can be replaced by F-domain spreading [15] using a spreading code. One of the advantages of using F-domain spreading instead of F-domain repetition in MC-DS-CDMA systems is that frequency diversity can be achieved without reducing the maximum number of users supported by the system [15, 16]. The MC-DS-CDMA scheme can provide the following advantages [13]. First, the spreading processing gain is increased compared to the corresponding single-carrier DS-CDMA scheme. Second, the effect of multipath interference is mitigated because of DS spreading. Third, frequency/time diversity can be achieved. Finally, a longer chip duration may lead to more relaxed synchronization schemes.

10.2.3 Time-Domain Spreading Multicarrier CDMA: MT-CDMA

The multitone CDMA (MT-CDMA) scheme was proposed by Vandendorpe in [17, 18]. The MT-CDMA transmitter spreads the serial-to-parallel converted data streams using a given spreading code in the time domain, so that the spectrum of each subcarrier prior to the spreading operation can satisfy the orthogonality condition with the minimum frequency separation [18]. Therefore, there exists a strong spectral overlap among the different subcarrier signals after DS spreading. The spectra associated with three subcarriers for an MT-CDMA signal are shown in Figure 10.1c. In an MT-CDMA system, the subcarrier frequencies are chosen to be orthogonal to each other with the minimum frequency separation before spreading, which can be formulated as

$$f_i - f_j = \frac{n|i-j|}{T_{MC}},$$

where $n \in \mathbb{N}$ and T_{MC} is the symbol duration after S/P. It can be shown that the minimum spacing of the subcarrier frequencies is $1/T_{MC}$.

Unfortunately, the MT-CDMA scheme suffers from intercarrier interference because of the strong spectral overlap among the different subcarriers. However, the capability to use longer spreading codes results in the reduction of self-interference and multiple access interference, compared to the spreading codes assigned to a corresponding single-carrier DS-CDMA scheme. The MT-CDMA scheme uses longer spreading codes than the corresponding single-carrier DS-CDMA scheme [2], where the relative code-length extension is in proportion to the number of subcarriers. Therefore, the MT-CDMA system can accommodate more users. Simulation results will later show the advantages of MT-CDMA in increasing throughput and bandwidth efficiency.

10.2.4 Multicarrier CDMA Transmitter Selection

We had briefly outlined the features of a number of multicarrier CDMA systems, which have been studied in the literature. So far, many reports are dedicated to the BER performance comparisons of DS-CDMA with multicarrier CDMA systems. These works show that all multicarrier CDMA schemes—MC-CDMA [19–21], MC-DS-CDMA [13, 14], and MT-CDMA [22]—outperform DS-CDMA.

In addition, it can be shown that there are trade-offs associated with each multicarrier CDMA scheme considered. Each technique has different benefits and drawbacks, depending on the intended applications [2, 14, 23]. Yang and Hanzo showed in [24] that MC-DS-CDMA has the highest degree of freedom in the family of CDMA schemes that can be beneficially exploited during the system design and reconfiguration procedures. The MC-DS-CDMA constitutes a trade-off between DS-CDMA and MC-CDMA in the context of the system's architecture and performance. By employing multiple subcarriers, MC-DS-CDMA typically requires lower-chip-rate spreading codes than DS-CDMA. It necessitates a lower number of subcarriers than MC-CDMA due to imposing DS

spreading on each subcarrier's signal. Consequently, MC-DS-CDMA typically requires lower-rate signal processing than DS-CDMA and has lower worst-case peak-to-average power fluctuation than MC-CDMA.

Therefore, we will study the MC-DS-CDMA–air interface in this chapter. In addition, we broaden our analysis by considering the family of generalized MC-DS-CDMA transceivers, defined in [4]. This generalized scheme includes the subclasses of MT-CDMA and MC-DS-CDMA as special cases. Simulation results will later show the advantages of MT-CDMA in increasing throughput and bandwidth efficiency.

In the following sections, we will adopt this general view and simply refer to it as MC-CDMA in the remainder of the chapter unless otherwise required. We also assume the uplink of an asynchronous multicellular multicarrier CDMA system with C in-cell active users. For the sake of simplicity, we assume that all users use the same subcarriers and transmit with the same modulation at the same rate.

10.2.5 MC-CDMA Transmission Model

This section explains in more detail the MC-CDMA scheme adopted in this chapter. The block diagram of the MC-CDMA transmitter is shown in Figure 10.2. The input information sequence of the u^{th} user is first converted into $N_c = 2K + 1$ parallel* data sequences $b^u_{-K,n}, \ldots, b^u_{0,n}, \ldots, b^u_{K,n}$, where n is the time index. The datum $b^u_{K,n} \in C_{\mathcal{M}}$ is $\mathcal{M}$-PSK modulated and differentially† encoded at rate $1/T_{MC}$, where $T_{MC} = N_c \times T$ is the symbol duration after S/P conversion, T is the symbol duration before S/P, and $C_{\mathcal{M}} = \{\ldots, e^{j2\pi m/\mathcal{M}}, \ldots\}$, $m \in \{0, \ldots, \mathcal{M} - 1\}$. The resulting S/P converter output is then spread with a random spreading code $c_u(t)$ at a rate $1/T_c$. The spreading factor, defined as the ratio between the chip rate and the symbol rate, is $\mathrm{L} = T_{MC}/T_c$. We write the spreading-code segment over the n^{th} period T_{MC} as

$$c^u_n(t) = \sum_{l=0}^{L-1} c^u_{l,n}\phi\left(t - lT_c - nT_{MC}\right), \tag{10.1}$$

where $c^u_{l,n} = \pm 1$ for $l = 0, \ldots, \mathrm{L} - 1$ is a random sequence of length L and $\phi(t)$ is the chip pulse. We consider square-root raised cosine chip pulses with roll-off factor β (see appendix). Closed-loop power control is taken into account at the transmitter by the amplification factor $a_u(t)$. All the data are then modulated in baseband by the inverse discrete Fourier transform (IDFT) and summed to obtain the multicarrier signal. No guard interval is inserted. Indeed, the channel identification and equalization are achieved by MC-STAR (multicarrier spatiotemporal array receiver) [32], and simulation results have shown that the guard interval length does not affect the link-level performance. MC-STAR exploits the intrinsic channel diversity by combining and equalizing the multipath signals. We

* We selected an odd number of subcarriers to have a central frequency, but the model can easily be rearranged to operate with an even number of subcarriers.

† We can also use pilot symbols for coherent modulation and detection [25], but that is beyond the scope of this chapter.

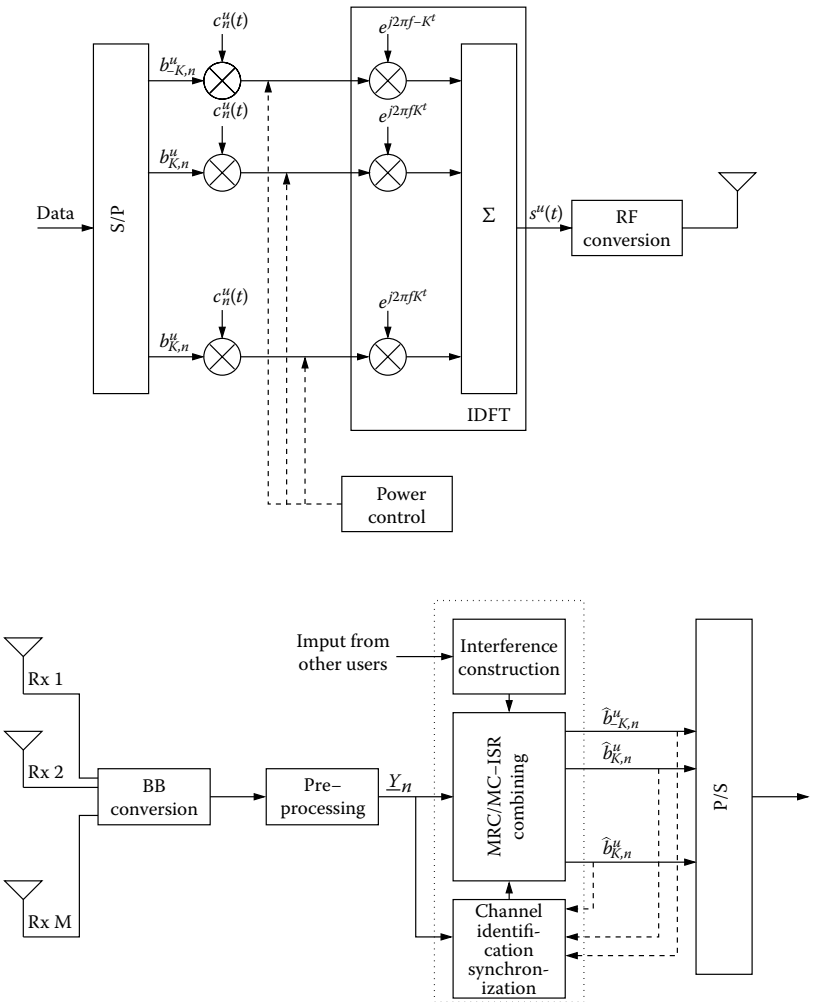

FIGURE 10.2 Block diagram of the MC-CDMA transmitter and receiver (pulse shape filtering is implemented at both transceiver ends).

hence eliminate the guard interval. Finally, the signal is transmitted after radio frequency upconversion.

The modulated subcarriers are orthogonal over the symbol duration T_{MC}. The frequency corresponding to the k^{th} subcarrier is $f_k = \lambda \times k/T_{MC}$. The transmitter belongs to the family of MT-CDMA if λ is set to 1, and to the class of MC-DS-CDMA if λ is set to L (see resulting signal spectra in Figure 10.3). Indeed, in an MT-CDMA system, the subcarrier frequencies are chosen to be orthogonal harmonics with minimum frequency separation before spreading. By contrast, in MC-DS-CDMA, the subcarrier frequencies are chosen to satisfy the orthogonality condition with minimum possible frequency after spreading. The transmitted signal of the u^{th} user is given by

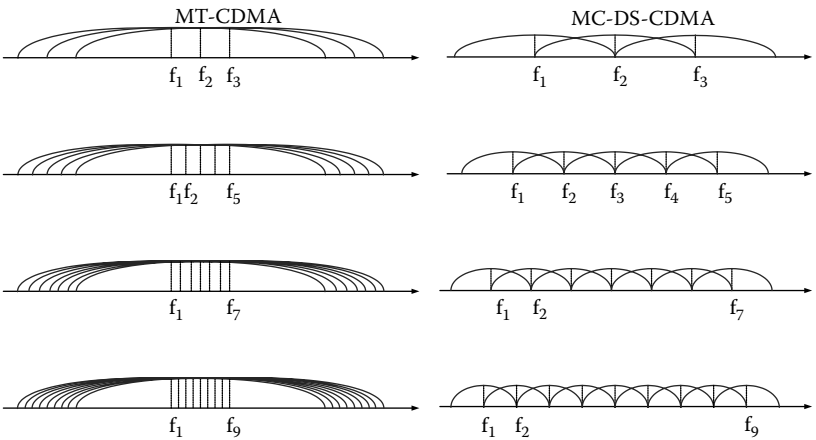

FIGURE 10.3 Different configurations of MT-CDMA and MC-DS-CDMA spectra within the same bandwidth.

$$s^u(t) = \sum_{k=-K}^{K} \sum_{n=-\infty}^{\infty} a^u(t) b_{k,n}^u c_n^u(t) e^{j2\pi f_k t}. \tag{10.2}$$

The transmitted signal's bandwidth is

$$BW = \frac{(N_c - 1)\lambda}{T_{MC}} + \frac{(1+\beta)}{T_c}. \tag{10.3}$$

10.2.6 Channel Model for Multicarrier Transmission

We consider an uplink transmission to M receiving antennas at the base station. The channel is assumed to be a slowly varying frequency-selective Rayleigh channel with delay spread $\Delta\tau$. For each k^{th} subcarrier of user u, the key channel parameter is the number of resolvable paths, P_k^u, which is given by

$$P_k^u = \left\lfloor \frac{\Delta\tau}{T_c} \right\rfloor + 1, \tag{10.4}$$

where T_c is the chip duration. In practice, the number of multipaths depends also on the choice of the noise threshold used to differentiate between the received multipath components and the thermal noise. Typical delay-spread values are in the range of 0.4–4 μs in outdoor mobile radio channels, and the number of multipaths P_k^u varies between 2 and 5 with 3.84 megachips per second (Mcps) resolution [26]. The M-dimensional

complex low-pass equivalent vector representation of the impulse response experienced by subcarrier k of the u^{th} user, for a receiver equipped with M antennas, is

$$H_k^u(t) = \frac{\rho_k^u(t)}{\left(r^u\right)^e(t)} \sum_{p=1}^{P_k^u} \mathcal{G}_{k,p}^u(t)\,\delta\left(t - \tau_{k,p}^u(t)\right). \tag{10.5}$$

where $\rho_k^u(t)$ and $(r^u)^e(t)$ model the effects of shadowing and path loss, respectively, $r^u(t)$ is the distance from the u^{th} user to the base station, and e is the path loss exponent. We assume their variations in time to be very slow, and hence nearly constant over several symbol durations. The M-dimensional complex vector $\mathcal{G}_{k,p}^u(t)$* denotes the fading and the array response from the user to the antenna elements of the receiver, and $\tau_{k,p}^u(t)$ represents the propagation time delay along the p^{th} path. We note here that the large-scale path loss that includes free-space path loss and shadowing is the same for all subcarriers of the same user. Moreover, the number of resolvable paths and their propagation time delays depend on the reflecting objects and scatterers and can be assumed equal for all subcarriers [28]. Therefore, we omit the index k from ρ, P, and τ ($\rho_k^u = \rho^u$, $P_k^u = P^u$, and $\tau_{k,p}^u = \tau_p^u$) and reformulate equation (10.5) as

$$H_k^u(t) = \frac{\rho^u(t)}{\left(r^u\right)^e(t)} \sum_{p=1}^{P^u} \mathcal{G}_{k,p}^u(t)\,\delta\left(t - \tau_p^u(t)\right). \tag{10.6}$$

A frequency-domain channel model for a multicarrier system can be characterized by the coherence bandwidth† [28]:

$$B_c \simeq \frac{1}{2\pi\Delta\tau}. \tag{10.7}$$

When the frequency separation λ/T_{MC} is less than B_C, the MC-CDMA system is subject to correlated fading over different subcarriers. Fades across taps (multipaths) are mutually independent for the same carrier. However, fading for the same tap across different carriers is correlated. The envelope correlation coefficient between subcarrier k and subcarrier k' for user u is [28]

$$\rho_{k,k'}^u = E\left[\left|\mathcal{G}_{k,p,m}^u(t)\right|\left|\mathcal{G}_{k',p,m}^u(t+\tau)\right|\right] = \frac{\left(1+\lambda_{k,k'}\right)\tilde{E}\left(\dfrac{2\sqrt{\lambda_{k,k'}}}{1+\lambda_{k,k'}}\right) - \dfrac{\pi}{2}}{2 - \dfrac{\pi}{2}}, \tag{10.8}$$

* We may characterize $\mathcal{G}_{k,p}^u(t)$ in a space manifold parameterized by angles of arrivals [27]. However, a space characterization requires perfect antenna calibration and adequate sensor positioning.

† The coherence bandwidth is defined as the bandwidth over which the envelope correlation is above 0.5 [28].

with

$$\lambda_{k,k'} = \frac{J_0\left(2\pi f_D \tau\right)}{\sqrt{1+\left[2\pi\left(f_k - f_{k'}\right)\Delta\tau\right]^2}}, \tag{10.9}$$

where E is the expectation function, $\mathcal{G}^u_{k,p,m}(t)$ is the fading and the antenna response from user u to antenna m of the receiver along the p^{th} path, $\tilde{E}$ is the complete elliptic integral of the second kind, J_0 is the zeroth-order Bessel function, and f_D is the maximum Doppler frequency. We adopt the approach proposed in [29, 30] to generate correlated Rayleigh channels across subcarriers. We also assume that the received channel multipath components across the M antennas are independent.

10.2.7 Received Signal

For a multicellular MC-CDMA system with C in-cell users and $N_c = 2K + 1$ carriers, the received signal is the superposition of signals from all users and all subcarriers. Hence, the M-dimensional observation vector received, after downconversion, by the antenna array can be expressed as follows:

$$\begin{aligned} X(t) &= \sum_{u=1}^{C}\sum_{k=-K}^{K}\sum_{n=-\infty}^{\infty} H^u_k(t) \otimes a^u(t) b^u_{k,n} c^u_n(t) e^{j2\pi(f_k+\Delta f^u)t} + N(t), \\ &= \sum_{u=1}^{C}\sum_{k=-K}^{K}\sum_{n=-\infty}^{\infty} X^u_{k,n}(t) + N(t), \end{aligned} \tag{10.10}$$

where $\otimes$ denotes time convolution and Δf^u models the carrier frequency offset (CFO), which is assumed equal for all subcarriers. This is a realistic assumption since there is only one oscillator per transmitter (see Figure 10.2). On the downlink, the CFO is even equal for all in-cell users (i.e., $\Delta f^u = \Delta f \ \forall\, u \in \{1, \ldots, C\}$). The noise term $N(t)$ includes the thermal noise received at the antennas as well as the out-cell interference. The contribution $X^u_{k,n}(t)$ of the n^{th} data symbol over the k^{th} carrier of user u to the received vector $X(t)$ is given by

$$\begin{aligned} X^u_{k,n}(t) &= H^u_k(t) \otimes a^u(t) b^u_{k,n} c^u_n(t) e^{j2\pi(f_k+\Delta f^u)t} \\ &= \psi^u_k(t) b_{k,n} \sum_{p=1}^{P^u} G^u_{k,p}(t) \varepsilon^u_{k,p}(t) c^u_n\left(t-\tau^u_p\right) e^{j2\pi(f_k+\Delta f^u)(t-\tau^u_p)}. \end{aligned} \tag{10.11}$$

Along the p^{th} path, $\mathcal{G}^u_{k,p}(t) = (\sqrt{M}/\|\mathcal{G}^u_{k,p}(t)\|)\mathcal{G}^u_{k,p}(t)$ is the propagation vector over the k^{th} subcarrier of the u^{th} user with norm $\sqrt{M}$, and $(\varepsilon^u_{k,p})^2(t) = \|\mathcal{G}^u_{k,p}(t)\|^2 / \sum_{p=1}^{P_u} \|\mathcal{G}^u_{k,p}(t)\|$ is the fraction of the total received power on the k^{th} subcarrier of user u:

$$\left(\psi_k^u\right)^2(t)=\left(\frac{\rho^u(t)}{\left(r^u\right)^e(t)}\right)^2\left(a^u\right)^2(t)\sum_{p=1}^{P^u}\frac{\left\|\mathcal{G}_{k,p}^u(t)\right\|^2}{M}. \tag{10.12}$$

10.2.8 Interference Analysis

We define the matched-filtered observation vector of frame number n over a time interval $[0, T_{MC})$ as

$$Y_n(t)=\frac{1}{T_c}\int_{D_\phi} X\left(nT_{MC}+t+t'\right)\phi(t')dt', \tag{10.13}$$

where D_ϕ denotes the temporal support* of $\phi(t)$. After sampling at a multiple of the chip rate, we frame the observation into overlapping blocks of constant length N_p. The oversampling ratio k_s is defined as the number of samples per chip. In DS-CDMA and MT-CDMA systems we need no more than one sample per chip ($k_s = 1$). In contrast, in an MC-DS-CDMA system, a higher sampling frequency is necessary for the receiver. Indeed, the sampling frequency has to satisfy the Nyquist sampling theorem, which states that the sampling interval must be smaller than the inverse of the double-sided bandwidth of the sampled signals. Hence, the smallest number greater than the number of subcarriers N_c is an adequate oversampling ratio for MC-DS-CDMA. The resulting processing block duration $T_P = N_P(T_c/k_s)$ is equal to $T_{max} + \overline{\Delta\tau}$. The processing period $T_{max} = LT_c$ contains N_c carrier symbols targeted for detection. The frame overlap $\overline{\Delta\tau} < T_{max}$, which is larger than the delay spread, allows multipath tracking [31]. Hence, we obtain the $M \times N_P$ matched-filtered observation matrix:

$$\mathbf{Y}_n=\left[Y_n(0), Y_n\left(T_c/k_s\right), \ldots, Y_n\left(\left(N_p-1\right)T_c/k_s\right)\right]. \tag{10.14}$$

It can be expressed as

$$\mathbf{Y}_n=\sum_{u=1}^{C}\sum_{k=-K}^{K}\sum_{n'=-\infty}^{\infty}\mathbf{Y}_{n',k,n}^u+N_n, \tag{10.15}$$

where the baseband preprocessed thermal noise and the out-cell interference contribute $\mathbf{N}_n$, and where symbol n' of carrier k of user u contributes its observation matrix $\mathbf{Y}_{n',k,n}^u$, obtained by

* For a rectangular pulse, D_ϕ is $[0, T_c]$. In practice, and as assumed in this chapter, it is the temporal support of a truncated square-root raised cosine, $D_\phi = [-N_{src}T_c, N_{src}T_c]$, where N_{src} stands for the truncation span of the shaping pulse in chip samples around 0.

$$\mathbf{Y}^{u}_{n',k,n}=\left[Y^{u}_{n',k,n}(0),Y^{u}_{n',k,n}\left(T_c/k_s\right),\ldots,Y^{u}_{n',k,n}\left(\left(\mathcal{N}_p-1\right)T_c/k_s\right)\right], \tag{10.16}$$

where

$$Y^{u}_{n',k,n}\left(t\right)=\frac{1}{T_c}\int_{D_\phi}X^{u}_{k,n'}\left(nT_{MC}+t+t'\right)\phi\left(t'\right)dt'. \tag{10.17}$$

As a result of the stationarity assumptions stated in section 10.2.6, $Y^{u}_{n',k,n}(t)$ can be developed into

$$\begin{aligned}Y^{u}_{n',k,n}\left(t\right)&\simeq e^{j2\pi\Delta f^{u}nT_{MC}}\psi^{u}_{k}\left(nT_{MC}\right)b^{u}_{k,n'}\frac{1}{T_c}\sum_{p=1}^{P}\int_{D_\phi}G^{u}_{k,p}\left(nT_{MC}+t+t'\right)\\&\quad\cdot\varepsilon^{u}_{k,p}\left(nT_{MC}+t+t'\right)e^{j2\pi f_k\left(nT_{MC}+t+t'+\tau^{u}_{p}\right)}c^{u}_{n'}\left(nT_{MC}+t+t'-\tau^{u}_{p}\right)\phi\left(t'\right)dt'\\&\simeq e^{j2\pi\Delta f^{u}nT_{MC}}\psi^{u}_{k}\left(nT_{MC}\right)b^{u}_{k,n'}V^{u}_{n',k,n}\left(t\right)\\&\simeq\psi^{u}_{k}\left(nT_{MC}\right)b^{u}_{k,n'}U^{u}_{n',k,n}\left(t\right),\end{aligned} \tag{10.18}$$

where the spread channel vector without CFO $V^{u}_{n',k,n}(t)$ is obtained by

$$V^{u}_{n',k,n}\left(t\right)=\frac{1}{T_c}\int_{D_\phi}H^{u}_{k}\left(nT_{MC}+t+t'\right)\otimes c^{u}_{n'}\left(nT_{MC}+t+t'\right)e^{j2\pi f_k\left(nT_{MC}+t+t'\right)}\phi\left(t'\right)dt', \tag{10.19}$$

and the spread channel vector is

$$U^{u}_{n',k,n}\left(t\right)=e^{j2\pi\Delta f^{u}nT_{MC}}V^{u}_{n',k,n}\left(t\right). \tag{10.20}$$

We assumed in the development of equation (10.18) that $\psi_k(nT_G + t + t')$ is constant during the interval $t' \in D_\phi$. We also considered that the frequency offset is small compared to the symbol rate ($\Delta f^{u}T_{MC} \ll 1$); thus, $e^{j2\pi\Delta f^{u}(nT_{MC}+t+t')} \simeq e^{j2\pi\Delta f^{u}nT_{MC}}$ for $t' \in D_\phi$ and $t \in [0, T_{MC})$. Substituting equation (10.18) in equation (10.15) gives

$$\begin{aligned}\mathbf{Y}_n&=\sum_{u=1}^{C}\sum_{k=-K}^{K}\sum_{n'=-\infty}^{\infty}b^{u}_{k,n'}\psi^{u}_{k,n}e^{j2\pi\Delta f^{u}nT_{MC}}\mathbf{V}^{u}_{n',k,n}+\mathbf{N}_n\\&=\sum_{u=1}^{C}\sum_{k=-K}^{K}\sum_{n'=-\infty}^{\infty}b^{u}_{k,n'}\psi^{u}_{k,n}\mathbf{U}^{u}_{n',k,n}+\mathbf{N}_n,\end{aligned} \tag{10.21}$$

where $\psi^{u}_{k,n} = \psi^{u}_{k}(nT_{MC})$. Due to asynchronism and multipath propagation, each user's carrier observation matrix carries information from the current as well as the previous and future symbols of the corresponding user's carrier. We therefore have

$$\mathbf{Y}_n = \sum_{u=1}^{C} \sum_{k=-K}^{K} \sum_{n'=n-1}^{n+1} b^u_{k,n'} \psi^u_{k,n} \mathbf{U}^u_{n',k,n} + \mathbf{N}_n. \tag{10.22}$$

Without loss of generality, let us focus on the detection of the n^{th} symbol carried by the k^{th} carrier of the desired user assigned index $d \in \{1, \ldots C\}$, i.e., $b^d_{k^d,n^d}$. Using equation (10.22) and defining a vector $\underline{V}$ as a matrix $\mathbf{V}$ reshaped column-wise, we can rewrite the observation matrix for a desired user d with respect to its n^{th} symbol of carrier k targeted for detection in the following simpler vector form:

$$\begin{aligned}
\underline{Y}_n &= \underbrace{s^d_{k,n} \underline{U}^d_{n,k,n}}_{\text{desired signal}} + \underbrace{\sum_{\substack{u=1 \\ u \neq d}}^{C} \sum_{k'=-K}^{K} \sum_{n'=n-1}^{n+1} s^u_{k',n'} \underline{U}^u_{n',k',n}}_{\underline{I}^d_{MAI,k,n}} \\
&+ \underbrace{\sum_{\substack{k'=-K \\ k' \neq k}}^{K} \sum_{n'=n-1}^{n+1} s^d_{k',n'} \underline{U}^d_{n',k',n}}_{\underline{I}^d_{\text{ICI},k,n}} + \underbrace{\sum_{\substack{n'=n-1 \\ n' \neq n}}^{n+1} s^d_{k,n'} \underline{U}^d_{n',k,n}}_{\underline{I}^d_{\text{ISI},k,n}} + \underline{N}_n, \\
&= s^d_{k,n} \underline{U}^d_{n,k,n} + \underline{I}^d_{k,n} + \underline{N}_n,
\end{aligned} \tag{10.23}$$

where $s^u_{k',n'} = \psi^u_{k',n} b^u_{k',n'}$ and $(\psi^u_{k,n})^2$ are the n'^{th} signal component of the k'^{th} carrier of user u, and the received power of user u over carrier k, respectively. The total interference $\underline{I}^d_{k,n}$ includes three types of interference: (1) the multiple access interference $\underline{I}^d_{\text{MAI},k,n}$ is the interference due to the N_c carriers from the other in-cell users $u \neq d$; (2) the inter-carrier interference $\underline{I}^d_{\text{ICI},k,n}$ is the interference due to the other carriers, $k' \neq k$, from the same user d; and (3) the intersymbol interference $\underline{I}^d_{\text{ISI},k,n}$ is the interference due to the same carrier k from the same user d. The noise vector $\underline{N}_n$, which comprises the pre-processed thermal noise and the interference due to out-of-cell users, is assumed to be uncorrelated both in space and time with variance σ^2_N.

In previous work [32], we proposed a receiver named MC-STAR. MC-STAR assumes the interference $\underline{I}^d_{k,n}$ as another contribution to the noise $\underline{N}_n$. Hence, the signal component of the desired user's carrier is extracted by spatiotemporal maximum ratio combining (MRC) as follows:

$$\hat{s}^d_{k,n} = \underline{W}^{d^H}_{MRC,k,n} \underline{Y}_n = \frac{\underline{\hat{U}}^{d^H}_{n,k,n} \underline{Y}_n}{\left\| \underline{\hat{U}}^d_{n,k,n} \right\|^2}, \tag{10.24}$$

where anywhere in the chapter the notation $\hat{\alpha}$ stands for an estimate of a given variable α, $(.)^H$ is the Hermitian operator, and $\underline{W}^d_{MRC,k,n}$ is the MRC beamformer. Equation (10.23)

shows that the net interference increases with the number of interferers and subcarriers, which severely limits the capacity of the MC-CDMA system with simple MRC receivers. Therefore, in the next section, we shall use the data decomposition of equation (10.23) to formulate the interference suppression problem and propose a new MC-CDMA receiver with full interference suppression capabilities.

10.2.9 Multiuser Detection Techniques for MC-CDMA Systems

Conventional multicarrier CDMA detectors—such as the matched filter, the RAKE combiner, and the MC-STAR receiver—are optimized for detecting the signal of a single desired user. RAKE combiners exploit the inherent multipath diversity in CDMA, since they essentially consist of matched filters for each resolvable path of the multipath channel. The outputs of these matched filters are then coherently combined according to a diversity combining technique, such as maximum ratio combining, equal gain combining, or selection diversity combining [13, 54]. Unlike RAKE-type receivers, which assume perfect knowledge of the channel [3], we proposed in previous work a full space-time receiver solution, named MC-STAR [43], that jointly implements adaptive channel identification and synchronization in both time and frequency.* These conventional single-user detectors are inefficient, because the interference is treated as noise and there is no utilization of the available knowledge about the mobile channel or the spreading sequences of the interferers.

In order to mitigate the problem of MAI, [33] proposed and analyzed the optimum multiuser detector for asynchronous Gaussian multiple access channels. This optimum detector significantly outperforms the conventional detector, and it is near–far resistant, but unfortunately its complexity grows exponentially with the number of interfering users. Following this work, numerous suboptimum multiuser detectors have been proposed for a variety of channels, data modulation schemes, and transmission formats. Since MC-CDMA systems also contain a DS-CDMA component, traditional suboptimum multiuser detection techniques can be performed on each carrier with some form of adaptation. A variety of linear multiuser receivers have been investigated for MC-CDMA systems such as the minimum mean square error (MMSE) detector [34] and the combination of MMSE and the decorrelator detector [35]. Interference cancellation (IC) schemes constitute another variant of multiuser detection that has been applied to MC-CDMA systems. They can be broadly divided into two categories: parallel cancellation (PIC) [37, 38] and successive cancellation (SIC) [36]. At each stage in the detector, the estimates of all the other users from the previous stage were used for reconstructing an estimate of the MAI, and this estimate was then subtracted from the interfered signal representing the wanted bit. A novel class of multicarrier multiuser detectors, referred to as subspace blind detectors, was proposed by [39] and [40], where only the spreading sequence and the delay of the desired user were known at the receiver. Based on this knowledge, a blind subspace tracking algorithm was developed for estimating the data of the desired user.

* MC-STAR is our starting receiver; hence, we will provide a short overview of this receiver in section 10.3.

Most of these multiuser receivers have focused on multiple access interference while ignoring the ICI. In addition, important system design issues such as carrier frequency offset recovery (CFOR) have often been neglected. In multiuser detection, the CFO of one user not only degrades the detection of that user itself, but also makes the receiver based on the ideal carrier frequency acquisition no longer optimal, thus degrading the detection of the other users [41]. An alternative multiuser detection technique, denoted interference subspace rejection (ISR), has been proposed for DS-CDMA [42]. This technique offers different modes. Each mode characterizes the interference vector in a different way and accordingly suppresses it. The flexibility and robustness inherent to ISR make its exploitation in multicarrier systems of great interest.

10.3 Proposed Adaptive Multicarrier CDMA Receiver: MC-ISR

This section is dedicated to the description, performance analysis, and implementation of the proposed MC-ISR receiver [6]. After a short overview of MC-STAR [43], which is our starting single-user receiver, we will describe and evaluate the adaptive interference rejection procedure that characterizes the proposed MC-ISR receiver.

10.3.1 The General Concept of MC-STAR

The adaptive receiver MC-STAR implements joint space-time-frequency processing over the despread data to improve the spectrum efficiency of the MC-CDMA system. The adaptive blind channel identification and equalization as well as the acquisition and tracking of multipaths and CFO are carried out on each subcarrier. However, their modules are interconnected to ensure proper information exchange and joint processing over carriers.* Mathematical details of the different adaptive procedures and their connections are provided in [43]. In this section, we explain the advantages of MC-STAR by describing the intermediate stages in our development that led to this receiver.

At the beginning, we extend original STAR, proposed for DS-CDMA [31], to a multicarrier system by placing STAR on each subcarrier. This extension requires a modification of the time-delay tracking procedure. Indeed, we introduce an intermediate transformation of the time response to reallow estimation of the multipath delays by simple linear regression.

Multi-carrier CDMA systems are very sensitive to the CFO. Therefore, we further introduce joint time-delay and frequency synchronization. The effect of the CFO on the performance of the spatiotemporal array receiver was not addressed in [31]. The space-time separation of the channel enables us to decouple time and carrier frequency synchronization. We can hence estimate the CFO by linear regression (LR) of the phase variation of each fading coefficient. Once an estimate of the carrier frequency offset

* The complexity of MC-STAR, which is approximately the complexity of STAR multiplied by the number of subcarriers, can be assessed using the results established in [44]. The latter suggests that MC-STAR can be implemented today on a single FPGA.

estimate $\widehat{\Delta f}$ is available by exploiting diversity in space, time, and frequency, we implement carrier frequency offset recovery (CFOR) in an adaptive closed-loop structure, where we feed back the estimate of the frequency offset to the input of the receiver. The CFOR reduces the time variations in the spatiotemporal propagation channel due to Δf to much weaker fluctuations due to the residual $\delta f = \Delta f - \widehat{\Delta f}$. It results in much weaker identification errors and enables further reduction of the carrier frequency estimation error δf.

At this stage, the receiver still consists of independent modules on each subcarrier. The purpose of the last step is to improve the performance of the overall receiver by interconnecting these modules and performing joint multicarrier processing. We exploit the intercarrier correlation, intrinsic to a multicarrier system, as a type of *frequency gain* to improve the performance by joint multicarrier channel identification and synchronization operations. Indeed, in the context of a multicarrier system, the adjacent subcarriers are exposed to correlated fading, especially if the delay spread of the channel is relatively low, resulting in relatively large coherence bandwidth. Hence, averaging the adjacent subcarrier channel parameters should improve the BER performance when transmitting over such low-dispersive fading channels. Along this perspective, the parameters common to all subcarriers can be estimated more accurately by averaging their estimates over all subcarriers. These parameters include the number of multipaths, their corresponding time delays, and the frequency offset. Other channel parameters, such as the channel fading coefficients, are correlated but not identical over all subcarriers. Therefore, combining them may not achieve the expected performance enhancement. We thus introduce a moving average technique over subcarriers with high correlation. The fact that subcarriers are highly correlated implies similar or identical channel parameters over subcarriers. Yet, the noise is uncorrelated across subcarriers, and hence the similar/common parameters can be estimated more accurately by averaging their estimates over all subcarriers, yielding the so-called frequency gain. The variance of the resulting estimation error is lower than the variance of the estimation error without frequency gain. Please bear in mind that we used the term *frequency gain* and not *frequency diversity*, which relies on the fact that the fading is different over different subcarriers.

10.3.2 Multicarrier Interference Subspace Rejection (MC-ISR)

Provided that an instantaneous estimate of the total interference $\hat{\underline{I}}^d_{k,n} = \hat{\underline{I}}^d_{\mathrm{MAI},k,n} + \hat{\underline{I}}^d_{\mathrm{ICI},k,n} + \hat{\underline{I}}^d_{\mathrm{ISI},k,n}$ is made available at the receiver (see section 10.3.4), we can eliminate it and yet achieve distortionless response to the desired signal by imposing the following simple constraints to the combiner $\underline{W}^d_{k,n}$:

$$\begin{cases} \underline{W}^{d^H}_{k,n}\hat{\underline{U}}^d_{n,k,n} & = 1, \\ \underline{W}^{d^H}_{k,n}\hat{\underline{I}}^d_{k,n} & = 0, \end{cases} \Rightarrow \begin{cases} \underline{W}^{d^H}_{\boldsymbol{k},n}\hat{\underline{U}}^d_{n,k,n} & = 1, \\ \underline{W}^{d^H}_{k,n}\left(\hat{\underline{I}}^d_{\mathrm{MAI},k,n} + \hat{\underline{I}}^d_{\mathrm{ICI},k,\boldsymbol{n}} + \hat{\underline{I}}^d_{\mathrm{ISI},k,n}\right) & = 0. \end{cases} \tag{10.25}$$

The first constraint guarantees a distortionless response to the desired signal, while the second directs a null to the total interference realization and thereby cancels it.

Exploiting the general framework developed in [42], the solution to the specific optimization problem in equation (10.25) is the MC-ISR combiner $\underline{W}_{k,n}^{d}$ given as follows:

$$\underline{W}_{k,n}^{d} = \frac{\Pi_{k,n}^{d} \underline{\hat{U}}_{n,k,n}^{d}}{\underline{\hat{U}}_{n,k,n}^{d^H} \prod_{k,n}^{d} \underline{\hat{U}}_{n,k,n}^{d}}, \tag{10.26}$$

$$Q_n = 1 \Big/ \left(\underline{\hat{I}}_{k,n}^{d^H} \underline{\hat{I}}_{k,n}^{d} \right) = 1 \Big/ \left\| \underline{\hat{I}}_{k,n}^{d} \right\|^2, \tag{10.27}$$

$$\mathbf{\Pi}_{k,n}^{d} = \mathbf{I}_{N_T} - \underline{\hat{I}}_{k,n}^{d} \underline{\hat{I}}_{k,n}^{d^H} \times Q_n, \tag{10.28}$$

where $N_T = M \times N_P$ is the total space dimension and $\mathbf{I}_{N_T}$ denotes an $N_T \times N_T$ identity matrix. First, we form the projector $\mathbf{\Pi}_{k,n}^{d}$ orthogonal to the total interference realization. Second, we project the estimated response vector $\underline{\hat{U}}_{n,k,n}^{d}$ and normalize it to derive the combiner. We use this combiner instead of MRC (used by MC-STAR) to extract the n^{th} signal component of the k^{th} carrier of the desired user as

$$\hat{s}_{k,n}^{d} = \underline{W}^{d^H}_{k,n} \underline{Y}_n. \tag{10.29}$$

Unlike most of the multiuser receivers proposed for MC-CDMA, which focus on multiple access interference while ignoring the intercarrier interference, MC-ISR fully suppresses the total interference resulting from MAI, ISI, and ICI by simple yet efficient nulling.* In addition, the interference suppression is made adaptive to track the current situation of the wireless channel and the interference. Simulation results will later show that ICI is not negligible and that full adaptive interference suppression is required to improve the MC-CDMA system performance.

10.3.3 Link/System-Level Performance Analysis

This section is dedicated to the performance analysis of the MC-ISR receiver based on the Gaussian assumption (GA). We exploit the analysis results of DS-CDMA ISR recently developed in [45] at the link level and extend them to MC-ISR. Additionally, we broaden the scope of the analysis to the system level.

10.3.3.1 Link-Level Performance

For the sake of simplicity, we assume temporarily perfect channel identification and perfect CFO estimation and recovery. Later in the simulations, we will use the channel

* The formulation of MC-ISR can be extended to MMSE-type criteria [42].

and CFO estimates provided by MC-STAR* [32]. The postcombined signal can be formulated as

$$\hat{s}^d_{k,n} = \underline{W}^{d\,H}_{k,n}\,\underline{Y}_n = s^d_{k,n} + \delta^d_{MAI,k,n} + \delta^d_{ICI,k,n} + \delta^d_{ISI,k,n} + \underline{W}^{d\,H}_{k,n}\,\underline{N}_n, \tag{10.30}$$

where $\delta^d_{MAI,k,n}$, $\delta^d_{ICI,k,n}$, and $\delta^d_{ISI,k,n}$ are the combining residuals of $\underline{I}^d_{\mathrm{MAI},k,n}$, $\underline{I}^d_{\mathrm{ICI},k,n}$, and $\underline{I}^d_{\mathrm{ISI},k,n}$, respectively. We assume here that the interference rejection residuals $\delta^d_{MAI,k,n}$, $\delta^d_{ICI,k,n}$, and $\delta^d_{ISI,k,n}$ are Gaussian random variables with zero mean. Hence, we only need to evaluate their variances. Note that the residuals would be null (i.e., $\delta^d_{MAI,k,n} = \delta^d_{ICI,k,n} = \delta^d_{ISI,k,n} = 0$) if the reconstruction of the interference were perfect (i.e., $\hat{\underline{I}}^d_{k,n} = \underline{I}^d_{k,n}$), and hence $\hat{s}^d_{k,n} = s^d_{k,n} + \underline{W}^{d\,H}_{k,n}\underline{N}_n$ would be corrupted only by the residual noise, which is Gaussian with zero mean and variance:

$$\mathrm{Var}\left[\underline{W}^{d\,H}_{k,n}\,\underline{N}_n\right] = \bar{\kappa}\sigma^2_N, \tag{10.31}$$

where

$$\bar{\kappa} = \mathrm{E}\left[\left\|\underline{W}^d_{k,n}\right\|^2\right] = \frac{ML-1}{ML-2},$$

is a measure of the enhancement of the white noise compared to MRC ($\bar{\kappa} = 1$ for MRC) [45]. However, in practice the interference vector is reconstructed erroneously due to wrong tentative data decisions and power control errors, and hence $\hat{s}^d_{k,n}$ is further corrupted by non-null residual interference rejection components. Therefore, we introduce the error indicating variables

$$\xi^u_{k,n} = \hat{b}^{u*}_{k,n} b^u_{k,n}$$

and

$$\lambda^u_{k,n} = \hat{\psi}^{u*}_{k,n}\,\psi^u_{k,n} \Big/ \left\|\hat{\psi}^u_{k,n}\right\|^2$$

where $(.)^*$ means complex conjugate. $\xi^u_{k,n}$ models the symbol estimation error provided by MRC at the initial stage. $\lambda^u_{k,n}$ characterizes the power control error. $\xi^u_{k,n}$ and $\lambda^u_{k,n}$ equal 1 when the estimated data symbol and the power control are perfect; otherwise, they are complex numbers. Since

$$\underline{Y}^u_{n',k',n} = s^u_{k',n'}\underline{U}^u_{n',k',n} = b^u_{k',n'}\psi^u_{k',n}\underline{U}^u_{n',k',n} = \xi^u_{k',n'}\lambda^u_{k',n}\hat{b}^u_{k',n'}\hat{\psi}^u_{k',n}\underline{U}^{\boldsymbol{u}}_{n',k'n} = \xi^u_{k',n'}\lambda^u_{k',n}\hat{\underline{Y}}^u_{n',k',n},\ \dagger$$

* Simulations will show little deviation from analysis in the operating BER region.

† Here we assume perfect time and frequency synchronization.

we can rewrite equation (10.23) as

$$\begin{aligned}\underline{Y}_n &= \underline{Y}^d_{n,k,n} + \sum_{\substack{u=1\\u\neq d}}^{C}\sum_{k'=-K}^{K}\sum_{n'=n-1}^{n+1}\xi^u_{k',n'}\lambda^u_{k',n}\hat{\underline{Y}}^u_{n',k',n} \\ &\quad + \sum_{\substack{k'=-K\\k'\neq k}}^{K}\sum_{n'=n-1}^{n+1}\xi^d_{k',n'}\lambda^d_{k',n}\hat{\underline{Y}}^d_{n',k',n} + \sum_{\substack{n'=n-1\\n'\neq n}}^{n+1}\xi^d_{k,n'}\lambda^d_{k,n}\hat{\underline{Y}}^d_{n',k,n} + \underline{N}_n.\end{aligned} \tag{10.32}$$

The signal after MC-ISR combining is then

$$\begin{aligned}\underline{W}^{dH}_{k,n}\underline{Y}_n &= s^d_{k,n} + \sum_{\substack{u=1\\u\neq d}}^{C}\sum_{k'=-K}^{K}\sum_{n'=n-1}^{n+1}\xi^u_{k',n'}\lambda^u_{k',n}\underline{W}^{dH}_{k,n}\hat{\underline{Y}}^u_{n',k',n} \\ &\quad + \sum_{\substack{k'=-K\\k'\neq k}}^{K}\sum_{n'=n-1}^{n+1}\xi^d_{k',n'}\lambda^d_{k',n}\underline{W}^{dH}_{k,n}\hat{\underline{Y}}^d_{n',k',n} + \sum_{\substack{n'=n-1\\n'\neq n}}^{n+1}\xi^d_{k,n'}\lambda^d_{k,n}\underline{W}^{dH}_{k,n}\hat{\underline{Y}}^d_{n',k,n} \\ &\quad + \underline{W}^{dH}_{k,n}\underline{N}_n.\end{aligned} \tag{10.33}$$

The MC-ISR combiner $\underline{W}^d_{k,n}$ satisfies the optimization property in equation (10.25), and thus

$$\underline{W}^{dH}_{k,n}\hat{\underline{I}}^d_{k,n} = 0 \;\Rightarrow\; \mathrm{Var}\left[\underline{W}^{dH}_{k,n}\left(\hat{\underline{I}}^d_{\mathrm{MAI},k,n} + \hat{\underline{I}}^d_{\mathrm{ICI},k,n} + \hat{\underline{I}}^d_{\mathrm{ISI},k,n}\right)\right] = 0. \tag{10.34}$$

This result allows the derivation of the variance of the interference rejection residuals, as shown in the appendix. Let $\bar{\psi}^2_D = E[(\bar{\psi}^d_k)^2]$ be the average power of the k^{th} carrier of the desired user and $\bar{\psi}^2_I$ be the average interference power on each interfering carrier. The variances of the residual $\underline{I}^d_{\mathrm{MAI},k,n}$ can be written as

$$\mathrm{Var}\left[\delta^d_{MAI,k,n}\right] = (C-1)\frac{\bar{\psi}^2_I}{L}\left[\varsigma(\beta) + \chi_k(\beta)\right](1+\rho_\lambda-\rho_\xi)\bar{\kappa}, \tag{10.35}$$

where $\varsigma(\beta) = 1 - \beta/4$ and

$$\chi_k(\beta) = \begin{cases}\dfrac{\beta}{8}, & \text{if } k = -K \text{ or } K,\\[2ex] \dfrac{\beta}{4}, & \text{if } k = -K+1, \ldots, K-1,\end{cases} \tag{10.36}$$

for MC-DS-CDMA ($\lambda = L$ and $f_k = k/T_c$) and

$$\chi_k(\beta)=\sum_{\substack{k'=-K\\k'\neq k}}^{K}\vartheta(|k-k'|), \tag{10.37}$$

where

$$\vartheta(x)=\begin{cases}1-\dfrac{\beta}{2}-\dfrac{x}{2L}+\dfrac{3\beta}{4\pi}\sin\left(\dfrac{\pi x}{\beta L}\right)+\left(\dfrac{\beta}{4}-\dfrac{x}{4L}\right)\cos\left(\dfrac{\pi x}{\beta L}\right), & \text{if } 0\le x/L\le\min(\beta,1-\beta)\\ 1-\dfrac{x}{L} & \text{if } \beta\le x/L\le 1-\beta \text{ and } \beta<0.5\\ \dfrac{3}{4}-\dfrac{\beta}{4}-\dfrac{x}{4L}+\dfrac{3\beta}{4\pi}\sin\left(\dfrac{\pi x}{\beta L}\right)+\left(\dfrac{\beta}{4}-\dfrac{x}{4L}\right)\cos\left(\dfrac{\pi x}{\beta L}\right)+ & \\ \quad\dfrac{3\beta}{8\pi}\sin\left(\dfrac{\pi x}{\beta L}-\dfrac{\pi}{\beta}\right)-\left(\dfrac{x}{8L}-\dfrac{1-\beta}{8}\right)\cos\left(\dfrac{\pi x}{\beta L}-\dfrac{\pi}{\beta}\right) & \text{if } 1-\beta\le x/L\le\beta \text{ and } \beta>0.5\\ \dfrac{3}{4}+\dfrac{\beta}{4}-\dfrac{3x}{4L}+\dfrac{3\beta}{8L}\sin\left(\dfrac{\pi x}{\beta L}-\dfrac{\pi}{\beta}\right)-\left(\dfrac{x}{8L}-\dfrac{1-\beta}{8}\right)\cos\left(\dfrac{\pi x}{\beta L}-\dfrac{\pi}{\beta}\right) & \text{if } \max(\beta,1-\beta)\le x/L\le 1\end{cases} \tag{10.38}$$

for MT-CDMA ($\lambda = L$ and $f_k = k/T_{Mc}$). The expressions of

$$\rho_\xi=\mathrm{E}\left[\xi^{u}_{k',n}\lambda^{u}_{k',n}\xi^{u'*}_{k',n}\lambda^{u'*}_{k',n}\right]$$

and

$$\rho_\lambda=\mathrm{E}\left[\left(\lambda^{u}_{k,n}\right)^2\right]-1$$

are derived for a Rayleigh fading channel with P paths to yield

$$\begin{aligned}\rho_\xi&=\left(1-\left(1-\cos\left(2\pi/\mathcal{M}\right)\right)S_{rec}\right)^2,\\ \rho_\lambda&=\frac{4\pi^2\left(f_D\times\tau_{PC}\right)^2}{P-1},\end{aligned} \tag{10.39}$$

where S_{rec} is the symbol error rate in the previous MC-ISR stage, f_D is the maximum Doppler frequency, and τ_{PC} is the power control feedback delay. The variances of the residuals $\underline{I}^{d}_{\mathrm{ICI},k,n}$ and $\underline{I}^{d}_{\mathrm{ISI},k,n}$ can be written as

$$\begin{aligned}\mathrm{Var}\left[\delta^{d}_{ICI,k,n}\right] &= \frac{\bar{\psi}_D^2}{L}\,\delta_{is}\chi_k(\beta)\left(1+\rho_\lambda-\rho_\xi\right)\bar{\kappa},\\ \mathrm{Var}\left[\delta^{d}_{ISI,k,n}\right] &= \frac{\bar{\psi}_D^2}{L}\,\delta_{is}\varsigma(\beta)\left(1+\rho_\lambda-\rho_\xi\right)\bar{\kappa},\end{aligned} \tag{10.40}$$

where $\delta_{is} = (P-1)/P$ is a measure of the relative impact of the interference generated by the other paths on a given path of the desired user (for a Rayleigh fading channel with P equal paths). The SINR on the k^{th} carrier can be estimated as

$$\mathrm{SINR}_{ISR,k} = \frac{\bar{\psi}_D^2}{\mathrm{Var}\left[\delta^{d}_{\mathrm{MAI},k,n}\right]+\mathrm{Var}\left[\delta^{d}_{\mathrm{ICI},k,n}\right]+\mathrm{Var}\left[\delta^{d}_{\mathrm{ISI},k,n}\right]+\bar{\kappa}\sigma_N^2}. \tag{10.41}$$

Note that the SINR expression above applies to MRC as well by setting $\bar{\kappa} = 1$ and $\rho_\lambda = \rho_\xi = 0$ in equations (10.35) and (10.40). Note also that in [46], we provide the variance of the interference for an MC-CDMA system with a rectangular pulse. In this chapter, we improve the analytical performance evaluation by deriving the variance of the interference with a more practical band-limited square-root raised cosine waveform. The BER performance on the k^{th} carrier is then given as follows:

$$P_e^k = \Omega\left(\mathrm{SINR}_{ISR,k}\right), \tag{10.42}$$

where Ω represents the single-user bound (SUB), which is classically defined as a conditional Gaussian Q-function over ψ_D and ψ_I. When using this classical representation, the average BER is derived by first finding the probability density functions (pdfs) of ψ_D and ψ_I and then averaging over those pdfs. Since it is difficult to find a simple expression for the pdfs of ψ_D and ψ_I that takes into consideration antenna diversity, imperfect power control, and imperfect channel identification, we may consider an approximative pdf. In this analysis, we choose to simulate Ω without imposing any pdf approximation. For each multicarrier configuration, we run single-user and single-carrier link-level simulations. We reproduced as much as possible most of the real-world operating conditions: time and frequency synchronization, imperfect power control, channel identification errors, antenna diversity, etc. These link-level simulations gave a realistic $\Omega : BER = \Omega(SNR)$. The simulations will later consider a multiuser and multicarrier environment. The average BER performance of the MC-ISR receiver is given by

$$P_e = \frac{1}{2K+1}\sum_{k=-K}^{K} P_e^k. \tag{10.43}$$

10.3.3.2 System-Level Performance

In order to compare the different MC-ISR configurations, the link-level curves provide a good picture of the performance of each system. But limiting comparisons to the

BER performance is not sufficient because the data rate is not equal for all configurations. Hence, we translate the link-level results into system-level results in terms of total throughput under the following three assumptions: (1) all users are received with an equal average power (i.e., $\bar{\psi}_D^2$ and $\bar{\psi}_I^2$) [4]; (2) all the cells have the same average load of C users per cell; and (3) the out-cell to in-cell interference ratio f is set to 0.6 [47]. Given these assumptions in an interference-limited system (thermal noise is low compared to interference), the link-level SIR at the base station antennas (ignoring ISI for simplicity) is

$$SIR_{ISR} = \frac{1}{(C-1)\alpha + \frac{1}{L}\delta_{is}\chi(\beta)(1+\rho_\lambda - \rho_\xi)\bar{\kappa} + Cf\lambda}, \tag{10.44}$$

where

$$\begin{aligned} \chi(\beta) &= \max_k\left[\chi_k(\beta)\right], \\ \alpha &= \frac{1}{L}\left(\varsigma(\beta)+\chi(\beta)\right)(1+\rho_\lambda-\rho_\xi)\bar{\kappa}, \\ \gamma &= \frac{1}{L}\left(\varsigma(\beta)+\chi(\beta)\right)\bar{\kappa}. \end{aligned} \tag{10.45}$$

$(C-1)\alpha$ is the normalized variance of the residual MAI ($u \neq d$), $\frac{1}{L}\delta_{is}\chi(\beta)(1+\rho_\lambda-\rho_\xi)\bar{\kappa}$ is the normalized variance of the residual ICI ($k' \neq k$ and $u = d$), and $Cf\gamma$ is the normalized variance of the out-cell interference. Note that equation (10.44) is derived from equation (10.41) and the assumption of negligible thermal noise and ISI.

The maximum number of users that can access the system C_{max} can be hence calculated by the simple procedure illustrated in Table 10.1. After initialization, this procedure increments the capacity C, until the SIR_{ISR} given by equation (10.44) no longer exceeds the required SNR_{req}. The SRN_{req} is the required SNR, derived from link-level simulations, to meet a BER of 5% in order to achieve a QoS of 10^{-6} after channel decoding. In step 2.2 of Table 10.1, we use the fact that the SIR expression applies to MRC by setting $\bar{\kappa} = 1$ and $\rho_\lambda = \rho_\xi = 0$ in equation (10.44). In step 2.3, we evaluate the symbol error rate S_{MRC} after the MRC stage as follows:

$$S_{MRC} = \Omega\left(\mathrm{SIR}_{MRC}\right), \tag{10.46}$$

where Ω represents the single-user bound (SUB). Note that multistage MC-ISR is considered in step 2.5. The total throughput is hence $\mathcal{T}_{max} = C_{max} \times R_b = C_{max} \times R_s \times \log_2(\mathcal{M})$ where R_b and R_s are the bit rate and symbol rate over all subcarriers, respectively.

10.3.4 MC-ISR Receiver Implementation

As mentioned in section 10.3.2, the proposed MC-ISR receiver requires accurate channel parameter estimates and data decisions to reconstruct the total interference $\hat{I}_{k,n}^{\mathrm{d}}$ and

TABLE 10.1 Capacity Computation Procedure

1. Initialize capacity $C = 0$.
2. Start computation loop:

2.1 Increment capacity $C = C + 1$.

2.2 Compute the SIR with MRC:

$$SIR_{MRC} = \frac{L}{(C-1)\left(\varsigma(\beta)+\chi(\beta)\right)+\chi(\beta)\delta_{is}+fC\left(\varsigma(\beta)+\chi(\beta)\right)}.$$

2.3 Compute the symbol error rate (SER) after MRC stage

$$S_{MRC} = \Omega\left(\mathrm{SIR}_{MRC}\right).$$

2.4 Compute ρ_λ and ρ_ξ.

2.5 Compute the SIR:

$$SIR_{ISR_1} = \frac{1}{(C-1)\alpha+\frac{1}{L}\delta_{is}\chi(\beta)\left(1+\rho_\lambda-\rho_\xi\right)\overline{\kappa}+Cf\gamma}.$$

If number of stages $S > 1$, start the loop; else go to 2.6.

For s = 2 : *S*.

Compute the symbol error rate (SER) after the $s - 1$ stage:

$$S_{ISR_{s-1}} = \Omega\left(\mathrm{SIR}ISR_{s-1}\right)$$

Compute ρ_ξ.

Compute the SIR:

$$SIR_{ISR_s} = \frac{1}{(C-1)\alpha+\frac{1}{L}\delta_{is}\chi(\beta)\left(1+\rho_\lambda-\rho_\xi\right)\overline{\kappa}+Cf\gamma}.$$

End.

2.6 If $SIR_{ISR_s} > SNR_{req}$ go to 2.1; else exit.

3. Decrement capacity $C = C - 1$.

null it reliably. Unlike previous works on interference suppression or multiuser detection [34, 38] that assume perfect knowledge of the channel, we propose here an adaptive receiver that uses runtime information about the channel and interference. Indeed, MC-ISR jointly implements channel identification and synchronization in both time and frequency, using MC-STAR [32], as well as signal combining with full interference suppression capabilities. Figure 10.2 shows the block diagram of the proposed receiver implementation, divided in four main modules. The first module is a preprocessor that downconverts the received signal to baseband, then passes it through the chip-matched filter before sampling and data block framing. The second module is a signal combiner that provides symbol estimates from the data observation, first by MRC in an initial iteration, then by MC-ISR in one or more iterative stages. The third module is an adaptive channel identifier and synchronizer from MC-STAR that implements closed-loop CFOR and estimates all the channel parameters (multipath time delays and their phases

and amplitudes, received power, CFO). The fourth module is a null-constraint generator common to all in-cell users. It gathers the data decisions and channel parameter estimates from the second and third modules dedicated to each in-cell user-carrier pair in order to reconstruct the total in-cell signal vector $\underline{I}_n$. Then to each combiner, say of the desired user-carrier pair as illustrated in Figure 10.1b, it passes on the associated null constraint (i.e., $\underline{I}^d_{k,n} = \underline{I}_n - s^d_{k,n}\underline{U}^d_{n,k,n}$) calculated with the least computations by simple subtraction from $\underline{I}_n$ of the desired signal contribution from the corresponding user-carrier pair.

The implementation of an adaptive closed-loop CFOR* jointly with multicarrier and multiuser detection (here by MC-ISR) requires careful attention regarding the order in which these two tasks should be processed. Indeed, conventional operation of CFOR at an early processing stage† prior to interference suppression would require (on the uplink only) as many independently CFO-compensated observations and interference null constraints as received in-cell users, thereby resulting in a tremendous complexity increase. Here we develop an efficient post-interference-suppression CFOR scheme by splitting the MC-ISR combining operation of equation (10.29) into two steps, an observation-cleaning projection and an MRC combining, and by inserting CFO compensation in between as follows:

$$\underline{Y}^d_{\Pi,k,n} = \Pi^d_{k,n}\underline{Y}_n, \tag{10.47}$$

$$\widehat{\Delta f}^d_n = \widehat{\Delta f}^d_{n-1} + \widehat{\delta f}^d_n, \tag{10.48}$$

$$\dot{\underline{Y}}^d_{\Pi,k,n} = \underline{Y}^d_{\Pi,k,n} e^{-j2\pi\widehat{\Delta f}^d_n nT}, \tag{10.49}$$

$$\hat{\underline{V}}^d_{\Pi,k,n} = \Pi^d_{k,n}\hat{\underline{V}}^d_{\Pi,k,n}, \tag{10.50}$$

$$\hat{s}^d_{k,n} = \frac{\hat{\underline{V}}^{d\,H}_{\Pi,k,n}\dot{\underline{Y}}^d_{\Pi,k,n}}{\left\|\hat{\underline{V}}^d_{\Pi,k,n}\right\|^2}. \tag{10.51}$$

The cleaning projection of equation (10.47) results in an almost interference-free observation $\underline{Y}^d_{\Pi,k,n}$ and allows for CFO estimation and compensation in equations (10.48) and (10.49), respectively, using the CFOR module of the single-user MC-STAR (refer to [32] and [48] for details on how to estimate the CFO adjustment term in equation (10.49)), and for MRC combining in equation (10.51) using the projected estimate of the

* In contrast to open-loop structures, closed-loop CFOR reduces the channel time variations and greatly improves their tracking [32].

† Usually CFOR is embedded in the RF chain or plugged to the preprocessor output.

spread channel vector without CFO $\hat{\underline{V}}^{d}_{\Pi,k,n}$. To the best of our knowledge, we are the first to report on and address this issue and to propose an efficient scheme for closed-loop CFOR in a multiuser detection context. It is important to mention here that if $\Delta f^{u} = \Delta f \ \forall \ u \in \{1, \ldots, C\}$ (i.e., downlink), then there is no need to estimate the CFO for the MC-ISR to null the in-cell interference. Indeed, the MC-ISR combiner $\underline{W}^{d}_{k,n}$ satisfies the optimization property in equation (10.25). Thus, it is not affected by the CFO of other users, i.e.,

$$\underline{W}^{d^H}_{k,n}\hat{\underline{I}}^{d}_{k,n} = 0 \ \Rightarrow \ e^{j2\pi\Delta f n T_{MC}}\left[\underline{W}^{d^H}_{k,n}\hat{\underline{I}}^{d}_{k,n}\right] = 0. \tag{10.52}$$

Once the MC-ISR projection is performed in equation (10.47) after reconstruction of $\hat{\underline{I}}^{d}_{k,n}$ without CFO, we implement the same CFOR scheme implemented in part by equations (10.48) and (10.49). Hence, like the near–far resistant detector proposed in [41], the multiuser CFOR problem can be transformed on the downlink into a single-user CFOR problem, and conventional single-user methods can therefore be used to estimate the frequency offset.*

To validate the efficiency of the proposed CFOR strategy in a multicarrier and multiuser detection scheme on the uplink, we consider a multiuser DBPSK MT-CDMA system with seven subcarriers, a spreading factor of 96, and five in-cell users ($N_c = 7$, $L = 96$, $C = 5$). We select the setup that will be introduced in section 10.4.1. The frequency offset normalized by the subcarrier separation ($\Delta f \times T_{MC}$) is set to 0.005 (i.e., $\Delta f = 200$ Hz).[15] Figure 10.4 shows the link-level results of MC-ISR with and without CFOR. Results suggest that a CFO of 200 Hz has a serious impact on the performance of MC-CDMA, and that the link-level gain with the proposed CFOR is in the range of 1 dB at a BER of 5% before channel decoding. By comparing the link-level curves of MC-ISR with CFOR and MC-ISR without a frequency offset (i.e., CFO=0 Hz), we notice that CFOR compensates almost completely the performance loss due to the frequency offset. These results confirm the need for and the efficiency of the proposed CFOR in a multicarrier and multiuser detection context.

10.4 Simulation Results

10.4.1 Simulation Setup

We consider an MC-CDMA system operating at a carrier of 1.9 GHz with maximum bandwidth of 5 MHz. We select a frequency offset Δf of 200 Hz, the maximum error tolerated by 3G standards† (≡ 0.1 ppm) for the frequency mismatch between the mobile and the base station [49]. We assume a frequency-selective Rayleigh fading channel with $P^{u} = P$ propagation paths with exponentially decreasing powers. The channel is

* The study of the CFOR performance is provided in [43].

† We select $\Delta f = 200$ Hz to show that even CFO residuals below the maximum value tolerated by 3G standards result in significant losses in performance.

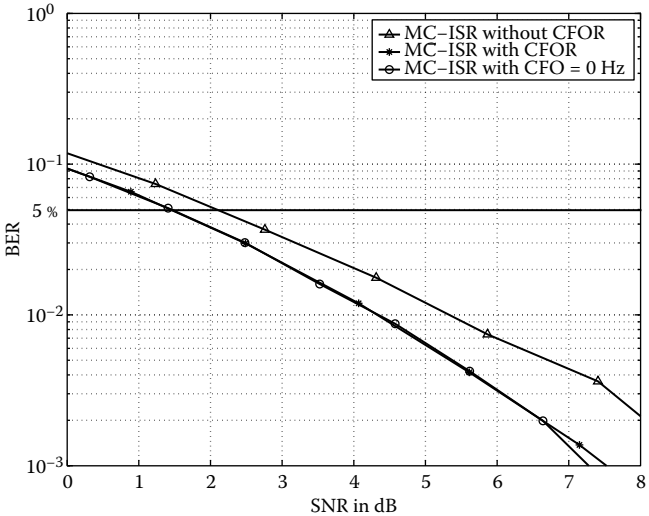

FIGURE 10.4 BER versus SNR for MT-CDMA MC-ISR, $L = 96$, $N_c = 7$, $C = 5$, with and without CFOR.

correlated across subcarriers and varying in time with Doppler shift f_D. We suppose a low Doppler situation $f_D = 8.8$ Hz unless otherwise mentioned. We consider that time delays vary linearly in time with a delay drift of 0.049 ppm. The receiver has $M = 2$ antennas. We implement closed-loop power control operating at 1,600 Hz and adjusting the power in steps of ±0.25 dB. An error rate on the power control bit of 5% and a feedback delay of 0.625 ms are simulated. The simulation parameters common to all multicarrier system configurations are listed in Table 10.2.

Table 10.3 shows the parameters specific to each multicarrier CDMA configuration. We choose as a reference the 3G DS-CDMA ($N_c = 1$) system with spreading factor $L = 32$ and a chip rate of 3.84 Mcps. We assume frequency-selective fading with $P = 3$ propagation paths. One of the features of MT-CDMA is that for a constant bandwidth the ratio between the spreading factor L and $2K = N_c - 1$ is constant. We hence maintain the same chip rate (3.840 Mcps) by changing the spreading factor and the number of subcarriers, as shown in Figure 10.3. We consider four MT-CDMA configurations. Since they use the same chip rate, there are three paths in each MT-CDMA subcarrier. For a fair comparison among different configurations of MC-DS-CDMA, the bandwidth should be the same. By reducing the chip rate, we varied the number of subcarriers while maintaining the orthogonality between them, as illustrated in Figure 10.3. Due to the reduction in bandwidth, each subcarrier in MC-DS-CDMA has either two paths (i.e., $P = 2$) or one path (i.e., $P = 1$, frequency-non-selective fading) for $N_c = 3$ and $N_c \geq 5$, respectively. The main performance criterion is the link-level SNR required per carrier to meet a BER of 5% in order to achieve a QoS of BER = 10^{-6} after channel decoding and the resulting system-level throughput. The user's data rate is calculated by summing the data rates over all subcarriers.

TABLE 10.2 Simulation Parameters

Parameter	Value	Comment
BW_{max}	5 MHz	Maximum bandwidth
M	2	Number of antennas
f_c	1.9 GHz	Central carrier frequency
f_D	8.8 Hz	Doppier frequency (5 kmph)
Δf	200 Hz	Frequency offset
f_{PC}	1,600 Hz	Frequency of PC updating
Δ_{PC}	±0.25 dB	Power control adjustment
PC_{min}^{max}	±30 dB	Power control stage
BER_{PC}	5%	Simulated PC bit error rate
$\delta\tau/\delta t$	0.049 ppm	Time-delay drift
$\Delta\tau$	4 chips	Delay spread
L_g	0	Guard interval length
N_s	2	Number of multistages
β	0.22	Roll-off factor
$2N_{src}+1$	9	Number of pulse samples

10.4.2 Validation of the Performance Analysis

In this section, we investigate the accuracy of the analytical performance analysis in section 10.3.3 under realistic channel conditions. Indeed, we do not assume perfect channel identification; instead, we use the channel estimate provided by MC-STAR [32]. We validate the Gaussian approximation (GA) of the residual interference by comparison with simulation results. Since the SUB (Ω) is not known explicitly in this case, it has been obtained from extensive simulations. We consider two configurations: DBPSK MT-CDMA (L=64, N_c = 3) and DBPSK MC-DS-CDMA (L=32, N_c = 3). Figure 10.5 shows the link-level performances. It is seen, not surprisingly, that the GA is accurate in the presence of moderate background noise. The accuracy of GA increases at larger loads or at lower Doppler situations (speed of V = 5 kmph). Despite the realistic channel model employed and the channel estimate errors, there is a very good match between the analytical and simulation results for both MT-CDMA and MC-DS-CDMA in the target BER region (5%). This suggests that the analytical evaluation is accurate in a low Doppler situation.

10.4.3 Advantage of Full Interference Suppression

The imperfect frequency downconversion due to the instability of local oscillators combined with the multipath effect destructs the subcarriers' orthogonality and hence causes ICI. In this section we evaluate the advantage of full interference suppression on the link-level performance of MC-CDMA. We plot the link-level performances of MT-CDMA (L = 64, N_c = 3, C = 8) and MC-DS-CDMA (L = 32, N_c = 3, C = 8) with MC-MRC (i.e., multicarrier receiver with MRC combining) and MC-ISR in Figure 10.6. It is clear that MC-ISR performs better than MC-MRC. Indeed, in low Doppler (speed of

TABLE 10.3 Parameters of Each Multicarrier System Configuration

Parameter	DS-CDMA	MT-CDMA					MC-DS-CDMA					Comment
λ	—	1					L					Subcarrier spacing parameter
N_c	1	3	5	7	9	11	3	5	7	9	11	Number of subcarriers
L	32	64	128	192	256	320	32	32	32	32	32	Spreading factor
R_c in Mcps	3.840	3.840	1.4549	0.8975	0.6488	0.5081	0.4175					Chip rate
P	3	3	2	1	1	1	1					Number of paths per subcarrier
R_s in kbaud	120	180	150	140	135	132	136.4	140.2	141.9	142.9	143.5	Symbol rate over all subcarriers
R_b for DBPSK in kbps	120	180	150	140	135	132	136.4	140.2	141.9	142.9	143.5	Peak rate of DBPSK
R_b for D8PSK in kbps	360	540	450	420	405	396	409.2	420.6	425.7	428.7	430.5	Peak rate for D8PSK
BW_{nor}	1	1.026	1									Bandwidth normalized vs. DS-CDMA

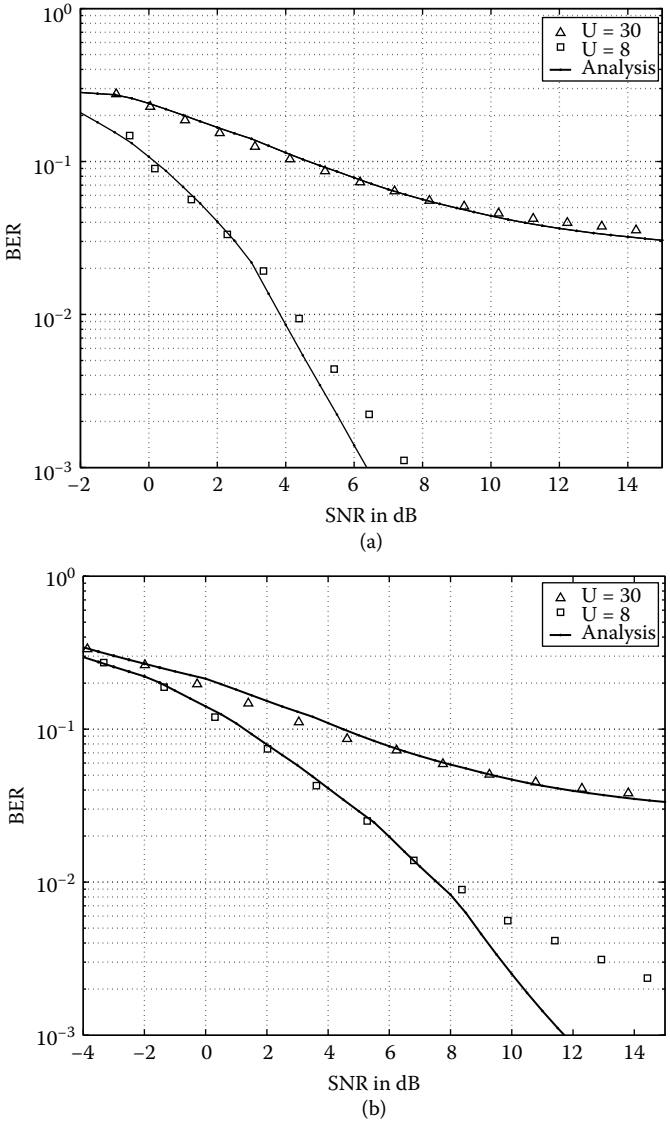

FIGURE 10.5 Analytical and simulated BER of MC-ISR versus SNR in dB for (a) MT-CDMA, $L = 64$, $N_c = 3$, DBPSK, and (b) MC-DS-CDMA $L = 32$, $N_c = 3$, DBPSK.

$V = 5$ kmph) we report 1.85 and 2 dB gains in SNR for MT-CDMA and MC-DS-CDMA, respectively. Note that the SNR gains are more important in high Doppler situations (speed of $V = 50$ kmph). At a bit error rate of 5%, MC-ISR performs 5.5 and 3 dB better than MC-MRC for MT-CDMA and MC-DS-CDMA, respectively.

In order to evaluate the specific impact of ICI on the link-level performance, we compare the BER curves of MT-CDMA ($L = 64$, $N_c = 3$, $C = 8$) MC-ISR with and without full

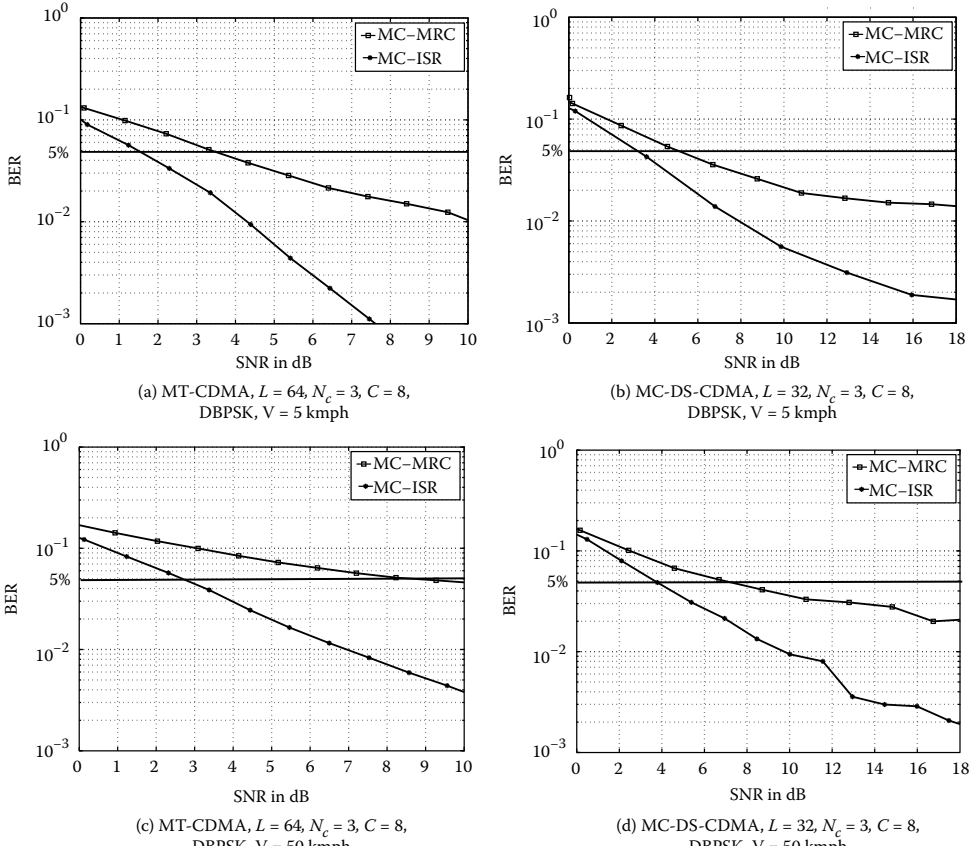

(a) MT-CDMA, $L = 64$, $N_c = 3$, $C = 8$, DBPSK, V = 5 kmph

(b) MC-DS-CDMA, $L = 32$, $N_c = 3$, $C = 8$, DBPSK, V = 5 kmph

(c) MT-CDMA, $L = 64$, $N_c = 3$, $C = 8$, DBPSK, V = 50 kmph

(d) MC-DS-CDMA, $L = 32$, $N_c = 3$, $C = 8$, DBPSK, V = 50 kmph

Figure 10.6 BER versus SNR in dB of MC-MRC and MC-ISR.

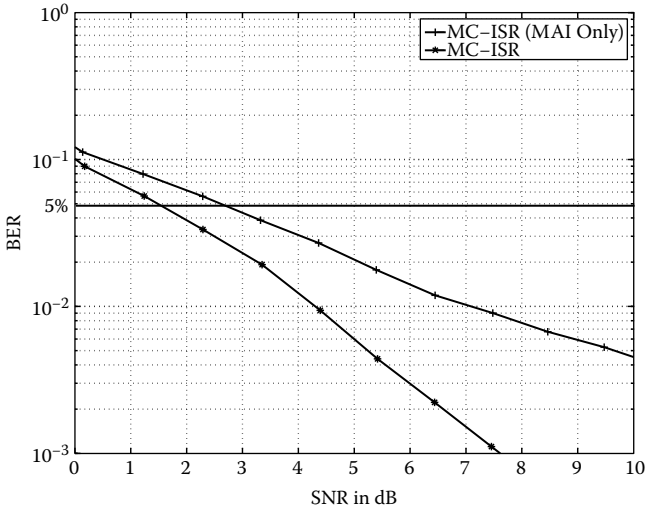

FIGURE 10.7 BER versus SNR in dB of MT-CDMA MC-ISR, $L = 64$, $N_c = 3$, $C = 8$, with and without full interference suppression (i.e., with and without ICI suppression).

interference suppression (i.e., with and without ICI suppression). Figure 10.7 shows that MC-ISR with full interference rejection is required to improve the system performance. Indeed, at a bit error rate of 5%, MC-ISR with full interference suppression performs 1.2 dB better than MC-ISR with MAI suppression only. In order to capture in more detail the gains achieved by ICI suppression in MC-CDMA, we proceed in Figure 10.8 to additional comparisons between the link-level BER performances of MC-ISR and MC-MRC in a single-user context (i.e., $C = 1$, no MAI, only ICI, and negligible ISI). Starting from the reference situation of Figure 10.8a with $L = 64$, $N_c = 7$, and DBSPK where the reported SNR gain due to ICI suppression is about 0.5 dB, the results suggest that ICI suppression is even more advantageous at higher-rate transmissions, and increasingly so when we move to the scenarios of Figures 10.8b–d; i.e., when we increase the number of carriers to $N_c = 11$ (SNR gain is about 1 dB), reduce the processing gain to $L = 32$ (SNR gain is about 3 dB), or increase the modulation order to D8PSK (SNR gain far exceeds 5 dB if not infinite), respectively. These results further confirm the benefits of ICI rejection in a full interference suppression scheme using MC-ISR.*

10.4.4 MT-CDMA, MC-DS-CDMA, and DS-CDMA Performance Comparison

This section is dedicated to the performance comparison of the proposed MC-ISR receiver with two potential next-generation multicarrier CDMA–air interface configurations: MT-CDMA and MC-DS-CDMA. Single-carrier ISR [42] for 3G DS-CDMA–air

* Simulation results performed in the framework of this contribution and reported in [50] show that the ICI rejection is even more beneficial in the case of one receiving antenna ($M = 1$).

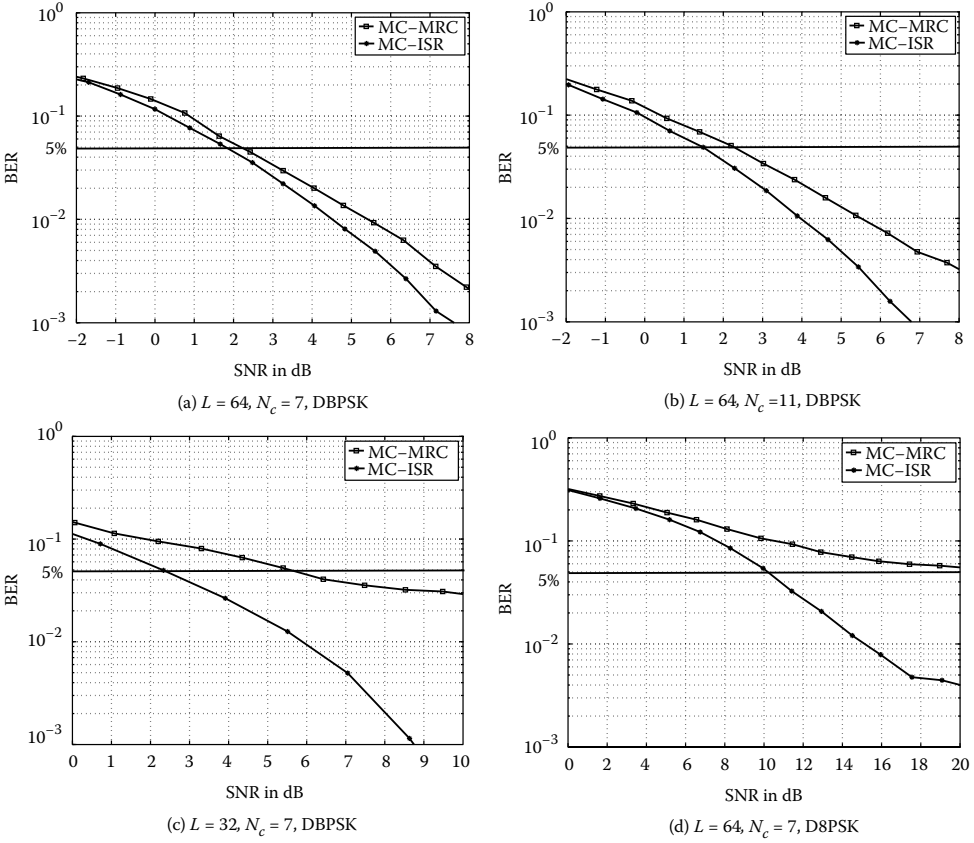

(a) $L = 64$, $N_c = 7$, DBPSK

(b) $L = 64$, $N_c = 11$, DBPSK

(c) $L = 32$, $N_c = 7$, DBPSK

(d) $L = 64$, $N_c = 7$, D8PSK

FIGURE 10.8 BER versus SNR in dB of MC-ISR and MC-MRC with single-user MT-CDMA.

interface is also considered as a reference. In addition, in order to provide a more detailed picture of the aggregate gain of the proposed MC-ISR receiver, we also compared its performance with that of MC-MRC over the same two multicarrier CDMA–air interface configurations, as well as with that of single-carrier MRC over current 3G DS-CDMA. First, we derive the SNR_{req} from link-level simulations. Then, we translate the link-level results into system-level results using the procedure in Table 10.1. In Table 10.4, we provide the required SNR and the total throughput of DBPSK and D8PSK modulated data for DS-CDMA, MT-CDMA, and MC-DS-CDMA. For DBPSK modulation, we observe that we can improve the system performance by increasing the number of subcarriers. Indeed, the total throughput continues to increase despite the increase in the number of carriers. But a gain saturation is encountered as the number of subcarriers increases. Note, however, that the throughput increase is more important with MC-ISR due to ICI suppression. Table 10.4 also shows that MT-CDMA outperforms MC-DS-CDMA with DBPSK modulation because it uses longer spreading sequences and exploits the subcarrier correlation. Moreover, due to the reduced subcarrier bandwidth, MC-DS-CDMA has less frequency diversity, while MT-CDMA is better able to exploit path diversity, and hence achieves better performance. Note also that MC-DS-CDMA is more robust against ICI, but in applying MC-ISR, this advantage over MT-CDMA becomes obsolete and the performance gap between MT-CDMA and MC-DS-CDMA increases.

Next, we compare different configurations with D8PSK modulation. We notice a link-level deterioration for MT-CDMA as the number of subcarriers increases. Indeed, higher-order modulation is more sensitive to the residual ICI. MC-DS-CDMA is much less affected by this phenomenon because it is much more robust to ICI thanks to the higher subcarrier spacing. Therefore, with high-order modulation, MC-DS-CDMA outperforms MT-CDMA when the number of subcarriers is high enough. We notice also that with the MC-MRC combiner, D8PSK MC-DS-CDMA outperforms D8PSK MT-CDMA even with a small number of subcarriers. It is clear, however, that D8PSK is less efficient than DBPSK modulation for all air interface configurations. In Table 10.4 we highlight the most spectrum-efficient MC-ISR–air interface configuration for each modulation. For both modulations MT-CDMA has the best link-level performance and the highest throughput (for a tested number of carriers less than or equal to 11). MT-CDMA with nine subcarriers and DBPSK modulation outperforms all other configurations and provides a throughput about 115% higher than that achievable with single-carrier MRC over a 3G DS-CDMA–air interface. The net benefits due to the proposed MC-ISR combiner and to the potential migration to a next-generation MT-CDMA–air interface are about 80 and 15%, respectively.

10.5 Conclusions

In this chapter we propose an adaptive multicarrier CDMA space-time receiver with full interference suppression capabilities named MC-ISR. First, we derived a complete model of the interference that takes into account MAI, ISI, and ICI in a multipath fading

TABLE 10.4 Required SNR and Maximum Throughput of DS-CDMA, MT-CDMA, and MC-CDMA for DBPSK and D8PSK (best performance values for each modulation are in bold)

MC-STAR Configuration	DS-CDMA	MT-CDMA					MC-DS-CDMA				
N_c	1	3	5	7	9	11	3	5	7	9	11
Modulation	DBPSK										
SNR_{req} in dB with MC-MRC	0.76	0.74	0.76	0.59	0.57	0.69	3.7	2.8	2.7	2.55	3
τ_{max} in kbps with MC-MRC	2,040	2,160	2,100	2,240	2,295	2,244	1091.2	1402	1419	1,571.9	1,435
SNR_{req} in dB with MC-ISR	0.76	0.74	0.75	0.55	0.5	0.62	3.62	2.8	2.6	2.48	3
τ_{max} in kbps with MC-ISR	3,600	3,960	4050	4,200	4,320	4,224	2,182.4	2,523.6	2,554.2	2,572.2	2,439.5
Modulation	DSPSK										
SNR_{req} in dB with MC-MRC	8.57	8	9.28	9	10	11	11	10.25	10.34	10.05	10.8
τ_{max} in kbps with MC-MRC	1,080	1,080	900	840	810	792	818.4	841.2	851.4	857.4	861
SNR_{req} in dB with MC-ISR	8.57	7.86	8.8	8.9	9.4	10.5	10.94	10.25	10.2	10.02	10.8
τ_{max} in kbps with MC-ISR	1,800	2,160	1,350	1,260	1,215	792	1,227.6	1,261.8	1,277.1	1,286.1	861

channel with timing and frequency mismatch. Based on this model, we proposed a new adaptive multicarrier interference subspace rejection receiver. We incorporated the least complex and more practical ISR interference rejection mode to simultaneously suppress MAI, ISI, and ICI at the signal combining step. We also proposed a realistic implementation of the new MC-ISR receiver that includes an efficient strategy for carrier offset recovery in a multicarrier and multiuser detection scheme. MC-ISR supports both the MT-CDMA– and MC-DS-CDMA–air interfaces. Furthermore, the assessment of the new MC-ISR receiver was oriented toward an implementation in a future, real-world wireless system. Indeed, we analyzed the performance of MC-ISR in an unknown time-varying Rayleigh channel with multipath, carrier offset, and cross-correlation between subcarrier channels and took into account all channel estimation errors. As another contribution in this work, we derived a link/system-level performance analysis of MC-ISR based on the Gaussian assumption (GA) and validated it by simulations. Under realistic propagation conditions and in the presence of channel estimation errors, simulation results validated the performance analysis and confirmed the net advantage of the full interference suppression capabilities of MC-ISR. With two receiving antennas and nine MT-CDMA subcarriers in 5 MHz bandwidth, MC-ISR provides about 4,320 kbps at low mobility for DBPSK, i.e., an increase of 115% in throughput over current 3G DS-CDMA with MRC.

Appendix

Derivation of the Interference Variance after MC-ISR Combining

Our goal is to estimate the variances:

$$\begin{aligned}\mathrm{Var}\left[\delta^{d}_{MAI,k,n}+\delta^{d}_{ICI,k,n}+\delta^{d}_{ISI,k,n}\right]=\mathrm{Var}\Bigg[&\sum_{\substack{u=1\\u\neq d}}^{C}\sum_{k'=-K}^{K}\sum_{n'=n-1}^{n+1}\xi^{u}_{k',n'}\lambda^{u}_{k',n}\underline{W}^{d^H}_{k,n}\hat{\underline{Y}}^{u}_{n',k',n}\\&+\sum_{\substack{k'=-K\\k'\neq k}}^{K}\sum_{n'=n-1}^{n+1}\xi^{d}_{k',n'}\lambda^{d}_{k',n}\underline{W}^{d^H}_{k,n}\hat{\underline{Y}}^{d}_{n',k',n}\\&+\sum_{\substack{n'=n-1\\n'\neq n}}^{n+1}\xi^{d}_{k,n'}\lambda^{d}_{k,n}\underline{W}^{d^H}_{k,n}\hat{\underline{Y}}^{d}_{n',k,n}\Bigg].\end{aligned}\tag{10.53}$$

Let us consider the general problem of deriving the variance of the sum of random complex variables. We first introduce the variables $x_\alpha, \alpha \in \{1, \ldots, N_t\}$ and $\xi_\alpha, \alpha \in \{1, \ldots, N_t\}$, with the following properties: $\mathrm{E}[\xi_\alpha \xi^*_{\alpha'}] = M_\xi, \forall \alpha \neq \alpha'$, $\mathrm{E}[\xi_\alpha \xi^*_\alpha] = V_\xi$, $\mathrm{E}[x_\alpha] = 0$, and $\mathrm{Var}[\sum_{\alpha=1}^{N_t} x_\alpha] = 0$. Then we assume that ξ_α and x_α are independent. Thus, we derive the variance as follows:

$$\begin{aligned}\mathrm{Var}\left[\sum_{\alpha=1}^{N_t}\xi_\alpha x_\alpha\right] &= \sum_{\alpha=1}^{N_t}\mathrm{Var}\left[\xi_\alpha x_\alpha\right]+\sum_{\alpha=1}^{N_t}\sum_{\alpha'=1\alpha'\neq\alpha}^{N_t}\mathrm{E}\left[\xi_\alpha\xi_{\alpha'}x_\alpha x_{\alpha'}\right]\\ &= \sum_{\alpha=1}^{N_t}V_\xi\mathrm{Var}\left[x_\alpha\right]+\sum_{\alpha=1}^{N_t}\sum_{\alpha'=1\alpha'\neq\alpha}^{N_t}\mathrm{E}\left[\xi_\alpha\xi_{\alpha'}\right]\mathrm{E}\left[x_\alpha x_{\alpha'}\right] \quad (10.54)\\ &= \sum_{\alpha=1}^{N_t}V_\xi\mathrm{Var}\left[x_\alpha\right]+\sum_{\alpha=1}^{N_t}\sum_{\alpha'=1\alpha'\neq\alpha}^{N_t}\rho_\xi\mathrm{E}\left[x_\alpha x_{\alpha'}\right].\end{aligned}$$

From $\mathrm{Var}[\sum_{\alpha=1}^{N_t} x_\alpha] = 0$ we have

$$\begin{aligned}\mathrm{Var}\left[\sum_{\alpha=1}^{N_t}x_\alpha\right] &= \sum_{\alpha=1}^{N_t}\mathrm{Var}\left[x_\alpha\right]+\sum_{\alpha=1}^{N_t}\sum_{\alpha'=1\alpha'\neq\alpha}^{N_t}\mathrm{E}\left[x_\alpha x_{\alpha'}\right]=0\\ &\Rightarrow \sum_{\alpha=1}^{N_t}\sum_{\alpha'=1\alpha'\neq\alpha}^{N_t}\mathrm{E}\left[x_\alpha x_{\alpha'}\right]=-\sum_{\alpha=1}^{N_t}\mathrm{Var}\left[x_\alpha\right].\end{aligned} \quad (10.55)$$

Then, by substituting equation (10.55) in equation (10.54) we obtain

$$\mathrm{Var}\left[\sum_{\alpha=1}^{N_t}\xi_\alpha x_\alpha\right]=\left(V_\xi-\rho_\xi\right)\sum_{\alpha=1}^{N_t}\mathrm{Var}\left[x_\alpha\right]. \quad (10.56)$$

Now we apply the same procedure to derive the variance of $\delta^d_{MAI,k,n} + \delta^d_{ICI,k,n} + \delta^d_{ISI,k,n}$. We substitute ξ_α with $\xi^u_{k',n'}\lambda^u_{k',n}$ and x_α with $\underline{W}^{d\,H}_{k,n}\underline{\hat{Y}}^u_{n',k'n}$. The MC-ISR combiner $\underline{W}^d_{k,n}$ satisfies the optimization property in equation (10.25); thus,

$$\underline{W}^{d\,H}_{k,n}\underline{\hat{I}}^d_{k,n}=0 \;\Rightarrow\; \mathrm{Var}\left[\underline{W}^{d\,H}_{k,n}\left(\underline{\hat{I}}^d_{\mathrm{MAI},,k,n}+\underline{\hat{I}}^d_{\mathrm{ICI},,k,n}+\underline{\hat{I}}^d_{\mathrm{ISI},,k,n}\right)\right]=0. \quad (10.57)$$

Then,

$$\begin{aligned}\mathrm{Var}\left[\delta^d_{MAI,k,n}+\delta^d_{ICI,k,n}+\delta^d_{ISI,k,n}\right] &= \left(V_\xi-\rho_\xi\right)\sum_{\substack{u=1\\u\neq d}}^{C}\sum_{k'=-K}^{K}\sum_{n'=n-1}^{n+1}\mathrm{Var}\left[\underline{W}^{d\,H}_{k,n}\underline{\hat{Y}}^u_{n',k',n}\right]\\ &+\left(V_\xi-\rho_\xi\right)\sum_{\substack{k'=-K\\k'\neq k}}^{K}\sum_{n'=n-1}^{n+1}\mathrm{Var}\left[\underline{W}^{d\,H}_{k,n}\underline{\hat{Y}}^d_{n',k',n}\right] \quad (10.58)\\ &+\left(V_\xi-\rho_\xi\right)\sum_{\substack{n'=n-1\\n'\neq n}}^{n+1}\mathrm{Var}\left[\underline{W}^{d\,H}_{k,n}\underline{\hat{Y}}^d_{n',k,n}\right].\end{aligned}$$

We consider $\mathrm{E}[\|\underline{W}_{k,n}^{d}\|^2] = \bar{\kappa}$, which is a measure of the enhancement of the white noise compared to the MRC combiner [45]. We also assume that the combiners $\underline{W}_{k,n}^{d}$ and $\hat{\underline{Y}}_{n',k'n}^{u}$ Thus, we derive the variance of the residual interference as follows:

$$\begin{aligned}\mathrm{Var}\left[\delta_{MAI,k,n}^{d}+\delta_{ICI,k,n}^{d}+\delta_{ISI,k,n}^{d}\right] &= \left(V_\xi-\rho_\xi\right)\bar{\kappa}\sum_{\substack{u=1\\u\neq d}}^{C}\sum_{k'=-K}^{K}\sum_{n'=n-1}^{n+1}\mathrm{Var}\left[\hat{\underline{Y}}_{n',k',n}^{u}\right]\\ &\quad+\left(V_\xi-\rho_\xi\right)\bar{\kappa}\sum_{\substack{k'=-K\\k'\neq k}}^{K}\sum_{n'=n-1}^{n+1}\mathrm{Var}\left[\hat{\underline{Y}}_{n',k',n}^{d}\right]\\ &\quad+\left(V_\xi-\rho_\xi\right)\bar{\kappa}\sum_{\substack{n'=n-1\\n'\neq n}}^{n+1}\mathrm{Var}\left[\hat{\underline{Y}}_{n',k,n}^{d}\right],\\ &=\left(V_\xi-\rho_\xi\right)\bar{\kappa}\,\mathrm{Var}\left[\hat{\underline{I}}_{k,n}^{d}\right].\end{aligned} \tag{10.59}$$

In the developments of equation (10.59), we exploited the fact that we transmit different data sequences over distinct subcarriers for a given user, and hence assumed that the cross-correlation terms from different subcarriers are zero.

In the following, we will derive the values of V_ξ and ρ_ξ under the following three assumptions: (1) the error indicating variables $\xi_{k',n'}^{u}$ and $\lambda_{k',n}^{u}$ are independent; (2) all the random sequence variables $(\xi_{k',n'}^{u})$ and $(\lambda_{k',n}^{u})$ are independent and identically distributed; and (3) $\mathrm{E}[\lambda_{k',n}^{u}]$. Given these assumptions we derive V_ξ as follows:

$$\begin{aligned}V_\xi &= \mathrm{E}\left[\xi_{k',n'}^{u}\lambda_{k',n}^{u}\xi_{k',n'}^{u^*}\lambda_{k',n}^{u^*}\right]=\mathrm{E}\left[\xi_{k',n'}^{u^*}\xi_{k',n'}^{u^*}\right]\mathrm{E}\left[\lambda_{k',n}^{u}\lambda_{k',n}^{u^*}\right]\\ &=\mathrm{E}\left[\lambda_{k',n}^{u}\lambda_{k',n}^{u^*}\right]=\left[1+\rho_\lambda\right].\end{aligned} \tag{10.60}$$

In order to evaluate V_ξ, we exploit the expression of the variance of the power control error in [51]. Hence, ρ_λ varies with the maximum Doppler frequency f_D (equation (10.51) in [51]), yielding:

$$\rho_\lambda = \frac{4\pi^2\left(F_D\times\tau_{PC}\right)^2}{P-1}, \tag{10.61}$$

where τ_{PC} is the power control feedback delay. Below we derive the expectation

$$\rho_\xi = \mathrm{E}\left[\xi_{k',n'}^{u}\lambda_{k',n}^{u}\xi_{k',n'}^{u'*}\lambda_{k',n}^{u'*}\right]=\mathrm{E}\left[\xi_{k',n'}^{u}\right]\mathrm{E}\left[\xi_{k',n'}^{u'*}\right]\mathrm{E}\left[\lambda_{k',n}^{u}\right]\mathrm{E}\left[\lambda_{k',n}^{u'*}\right]=\mathrm{E}\left[\xi_{k',n'}^{u}\right]^2.$$

If $S_{rec} \ll 1$, the value of ρ_ξ can be derived as follows [45]:

$$\rho_\xi \simeq \left(1-\left(1-\cos\left(2\pi/\mathcal{M}_t\right)\right)S_{rec}\right)^2. \tag{10.62}$$

The interference $\underline{I}_{k,n}^{d}$ is approximated as a Gaussian distributed random variable with zero mean. Only its variance needs to be evaluated to derive the variance of the residual interference in equation (10.59).

Derivation of the Interference Variance for Band-Limited MC-CDMA

The chip waveform has been noted to be an important system parameter for DS-CDMA and MC-DS-CDMA. Hence, the performances of DS-CDMA and MC-DS-CDMA with various time-limited and band-limited chip waveforms have been investigated. However, for all the MT-CDMA systems found in the literature, a time-limited waveform is generally employed [4, 18, 52, 53]. Since we consider a practical square-root raised cosine pulse, the focus of this appendix is to derive the variance of the interference of MC-CDMA (including MC-DS-CDMA and MT-CDMA) with a band-limited square-root raised cosine waveform. Let $G(f)$ be the Fourier transform of the raised cosine filter:

$$G(f)=\begin{cases} T_c, & 0\le|f|\le\dfrac{1-\beta}{2T_c} \\ \dfrac{T_c}{2}\left\{1+\cos\left[\dfrac{\pi T_c}{\beta}\left(|f|-\dfrac{1-\beta}{2T_c}\right)\right]\right\}, & \dfrac{1-\beta}{2T_c}\le|f|\le\dfrac{1+\beta}{2T_c} \\ 0, & |f|>\dfrac{1+\beta}{2T_c} \end{cases}. \tag{10.63}$$

Let $\bar{\psi}_D^2 = E[(\psi_k^d)^2]$ be the average power of the k^{th} carrier of the desired user and $\bar{\psi}_I^2$ be the average power on each interfering carrier (assumed equal for all u and all k). Using the general results in [54], one has

$$\mathrm{Var}\left[\underline{I}_{MAI,k,n}^{d}\right]=(C-1)\frac{\bar{\psi}_I^2}{L}\left[\varsigma(\beta)+\chi_k(\beta)\right], \tag{10.64}$$

where

$$\varsigma(\beta)=\frac{1}{T_c}\int_{-\infty}^{\infty}G^2(f)\,df \tag{10.65}$$

and

$$\chi_k(\beta)=\sum_{\substack{k'=-K\\k'\neq k}}^{K}\frac{1}{T_c}\int_{-\infty}^{\infty}G(f)G\left(f-\left(f_k-f_{k'}\right)\right)df\,. \tag{10.66}$$

It is easy to obtain $\varsigma(\beta) = 1 - \beta/4$). To obtain $\chi_k(\beta)$, we need to consider the MC-DS-CDMA and MT-CDMA systems separately. After mathematical evaluations of the integral, we obtain:

$$\chi_k(\beta) = \begin{cases} \dfrac{\beta}{8}, & \text{if } k = -K \text{ or } K, \\ \dfrac{\beta}{4}, & \text{if } k = -K+1, \ldots, K-1, \end{cases} \tag{10.67}$$

for MC-DS-CDMA ($\lambda = L$ and $f_k = k/T_c$) and

$$\chi_k(\beta) = \sum_{\substack{k'=-K \\ k' \neq k}}^{K} \vartheta\left(\left|k - k'\right|\right), \tag{10.68}$$

where

$$\vartheta(x) = \begin{cases} 1 - \dfrac{\beta}{2} - \dfrac{x}{2L} + \dfrac{3\beta}{4\pi}\sin\left(\dfrac{\pi x}{\beta L}\right) + \left(\dfrac{\beta}{4} - \dfrac{x}{4L}\right)\cos\left(\dfrac{\pi x}{\beta L}\right), & \text{if } 0 \le x/L \le \min(\beta, 1-\beta) \\ 1 - \dfrac{x}{L} & \text{if } \beta \le x/L \le 1-\beta \text{ and } \beta < 0.5 \\ \dfrac{3}{4} - \dfrac{\beta}{4} - \dfrac{x}{4L} + \dfrac{3\beta}{4\pi}\sin\left(\dfrac{\pi x}{\beta L}\right) + \left(\dfrac{\beta}{4} - \dfrac{x}{4L}\right)\cos\left(\dfrac{\pi x}{\beta L}\right) + & \\ \quad \dfrac{3\beta}{8\pi}\sin\left(\dfrac{\pi x}{\beta L} - \dfrac{\pi}{\beta}\right) - \left(\dfrac{x}{8L} - \dfrac{1-\beta}{8}\right)\cos\left(\dfrac{\pi x}{\beta L} - \dfrac{\pi}{\beta}\right) & \text{if } 1-\beta \le x/L \le \beta \text{ and } \beta > 0.5 \\ \dfrac{3}{4} + \dfrac{\beta}{4} - \dfrac{3x}{4L} + \dfrac{3\beta}{8L}\sin\left(\dfrac{\pi x}{\beta L} - \dfrac{\pi}{\beta}\right) - \left(\dfrac{x}{8L} - \dfrac{1-\beta}{8}\right)\cos\left(\dfrac{\pi x}{\beta L} - \dfrac{\pi}{\beta}\right) & \text{if } \max(\beta, 1-\beta) \le x/L \le 1 \end{cases} \tag{10.69}$$

for MT-CDMA ($\lambda = L$ and $f_k = k/T_{Mc}$). The variances of the residual ICI and ISI interferences from the same user can be written as

$$\begin{aligned} \mathrm{Var}\left[I^{d}_{ICI,k,n}\right] &= \frac{\bar{\Psi}_D^2}{L}\delta_{is}\chi_k(\beta), \\ \mathrm{Var}\left[I^{d}_{ISI,k,n}\right] &= \frac{\bar{\Psi}_D^2}{L}\delta_{is}\varsigma(\beta), \end{aligned} \tag{10.70}$$

where $\delta_{is} = (P - 1)/P$ is a measure of the relative impact of the interference generated by the other paths on a given path of the desired user.

References

[1] L. Hanzo, T. Killer, M. S. Munster, and B. J. Choi. 2003. *OFDM and MC-CDMA for broadband multiuser communications, WLANs and broadcasting*. New York: John Wiley & Sons.

[2] S. Hata and R. Prasad. 1997. Overview of multicarrier CDMA. *IEEE Commun. Mag.* 35:126–33.

[3] L. Hanzo, L.-L. Yang, E.-L. Kuan, and K. Yen. 2003. *Single- and multi-carrier CDMA multi-user detection, space-time spreading, synchronisation and standards*. New York: John Wiley & Sons.

[4] Y. Lie-Liang and L. Hanzo. 2002. Performance of generalized multicarrier DS-CDMA over Nakagami-m fading channels. *IEEE Trans. Commun.* 50:956–66.

[5] H. Steendam and M. Moeneclaey. 2001. The effect of carrier frequency offsets on downlink and uplink MC-DS-CDMA. *IEEE J. Selected Areas Commun.* 19:2528–36.

[6] B. Smida, S. Affes, K. Jamaoui, and P. Mermelstein. 2008. A multicarrier-CDMA space-time receiver with full interference suppression capabilities. *IEEE Trans. Veh. Technol.* 57(1):363–379.

[7] N. Yee, J. P. Linnarz, and G. Fettweis. 1993. Multi-carrier CDMA in indoor wireless radio networks. In *Proceedings of the IEEE International Symposium on Personal, Indoor and Mobile Radio Communications (PIMRC 1993)*, pp. 109–13.

[8] A. Chouly, A. Brajal, and S. Jourdan. 1993. Orthogonal multicarrier techniques applied to direct sequence spread spectrum CDMA systems. In *Proceedings of the IEEE Global Telecommunications Conference (GLOBECOM 1993)*, vol. 3, pp. 1723–28.

[9] K. Fazel and L. Papke. 1993. On the performance of convolutionally-coded CDMA/OFDM for mobile communication system. In *Proceedings of the IEEE Personal, Indoor and Mobile Radio Communications Symposium (PIMRC 1993)*, pp. 468–72.

[10] A. Chouly, A. Brajal, and S. Jourdan. 1993. Orthogonal multicarrier technique applied to direct sequence spread spectrum CDMA systems. In *Proceedings of the IEEE GLOBECOM '93*, pp. 1723–28.

[11] V. DaSilva and E. S. Sousa. 1993. Performance of orthogonal CDMA codes for quasi-synchronous communication systems. In *Proceedings of the IEEE International Conference on Universal Personal Communications (ICUPC 1993)*, vol. 2, pp. 995–99.

[12] S. Kondo and L. B. Milstein. 1993. On the use of multicarrier direct sequence spread spectrum systems. In *Proceedings of the IEEE Military Communinations Conference (MILCOM 1993)*, vol. 1, pp. 52–56.

[13] E. A. Sourour and M. Nakagawa. 1996. Performance of orthogonal multicarrier CDMA in a multipath fading channel. *IEEE Trans. Commun.* 44:356–67.

[14] X. Gui and T. S. Ng. 1999. Performance of asynchronous orthogonal multicarrier CDMA system in frequency selective fading channel. *IEEE Trans. Commun.* 47:1084–91.

[15] L. L. Yang and L. Hanzo. 2002. Broadband MC DS-CDMA using space-time and frequency-domain spreading. In *Proceedings of the IEEE VTC'2002*, pp. 1632–36.

[16] Z. Luo, J. Liu, M. Zhao, Y. Liu, and J. Gao. 2006. Double-orthogonal coded space-time-frequency spreading CDMA scheme. *IEEE J. Selected Areas Commun.* 24:1244–55.

[17] L. Vandendorpe. 1993. Multitone direct sequence CDMA system in an indoor wireless environment. In *Proceedings of the IEEE First Symposium on Communications and Vehicular Technology in the Beneluz*, pp. 4.1.1–4.1.8.

[18] L. Vandendorpe. 1995. Multitone spread spectrum multiple access communications system in a multipath Rician fading channel. *IEEE Trans. Veh. Technol.* 44:327–37.

[19] S. Kaiser. 1995. OFDM-CDMA versus DS-CDMA: Performance evaluation for fading channels. In *Proceedings of the IEEE International Conference on Communications (ICC 1995)*, vol. 3, pp. 1722–26.

[20] J.-Y. Oh and M.-S. Lim. 1999. The bandwidth efficiency increasing method of multi-carrier CDMA and its performance evaluation in comparison with DS-CDMA with RAKE receivers. In *Proceedings of the IEEE Vehicular Technology Conference (VTC 1999)*, vol. 1, pp. 561–65.

[21] S. B. Slimane. 1999. Bandwidth efficiency of MC-CDMA signals. *IEEE Electronics Lett.* 35:1797–98.

[22] X. Zhang, T.-S. Ng, and J. Wang. 1999. Capacity comparison of single-tone and multitone CDMA systems. In *Proceedings of the IEEE Vehicular Technology Conference (VTC 1999)*, vol. 1, pp. 243–47.

[23] S. Hata and R. Prasad. 1996. An overview of multi-carrier CDMA. In *Proceedings of the IEEE International Symposium on Spread Spectrum Techniques and Applications*, vol. 1, pp. 107–14.

[24] L. L. Yang and L. Hanzo. 2003. Multicarrier DS-CDMA: A multiple access scheme for ubiquitous broadband wireless communications. *IEEE Commun. Mag.* 41:116–24.

[25] S. Affes and P. Mermelstein. 2003. Adaptive space-time processing for wireless CDMA. In *Adaptive signal processing: Application to real-world problems*, ed. J. Benesty and A. H. Huang. Berlin: Springer, chapter 10.

[26] 3GPP. 1997. *Universal Mobile Telecommunications System (UMTS); Selection procedures for the choice of radio transmission technologies of the UMTS*. 3GPP TR 101 112 V3.1.0.

[27] S. Affes, D. Feng, L. Ge, and P. Mermelstein. 2002. Does direction-of-arrival estimation help channel identification in multi-antenna CDMA receivers? In *IEEE ISWC'2002*, pp. 167–68.

[28] W. C. Jakes, ed. 1974. *Microwave mobile communications*. New York: Wiley.

[29] B. Natarajan, C. R. Nassar, and V. Chandrasekhar. 2000. Generation of correlated Rayleigh fading envelopes for spread spectrum applications. *IEEE Commun. Lett.* 4:9–11.

[30] R. B. Ertel and J. H. Reed. 1998. Generation of two equal power correlated Rayleigh fading envelopes. *IEEE Commun. Lett.* 2:276–78.

[31] S. Affes and P. Mermelstein. 1998. A new receiver structure for asynchronous CDMA: STAR the spatio-temporal array-receiver. *IEEE J. Selected Areas Commun.* 16:1411–22.

[32] B. Smida, S. Affes, J. Li, and P. Mermelstein. 2005. Multicarrier-CDMA STAR with time and frequency synchronization. In *IEEE ICC 2005*, vol. 4, pp. 2493–99.

[33] S. Verdu. 1986. Minimum probability of error for asynchronous Gaussian multiple access channels. *IEEE Trans. Information Theory* 32:85–96.

[34] X. Weiping and L. B. Milstein. 1998. MMSE interference suppression for multicarrier DS-CDMA in frequency selective channels. In *IEEE GLOBECOM 1998*, vol. 1, pp. 259–64.

[35] H. Lie-Liang, H. Wei, and L. Hanzo. 2003. Multiuser detection in multicarrier CDMA systems employing both time-domain and frequency-domain spreading. In *IEEE PIMRC 2003*, vol. 2, pp. 1840–44.

[36] F. Lin and L. B. Milstein. 2000. Successive interference cancellation in multicarrier DS/CDMA. *IEEE Trans. Commun.* 48:1530–40.

[37] W. Huahui, K. W. Ang, K. Yen, and Y. H. Chew. 2003. An adaptive PIC receiver with diversity combining for MC-DS-CDMA system. In *IEEE VTC 2003*, vol. 2, pp. 1055–59.

[38] W. Huahui, K. W. Ang, K. Yen, and Y. H. Chew. 2000. Performance analysis of an adaptive PIC receiver for asynchronous multicarrier DS-CDMA system. In *IEEE PIMRC 2003*, vol. 2, pp. 1835–39.

[39] W. Nabhane and H. V. Poor. Blind joint equalization and multiuser detection in dispersive MCCDMA/MC-DS-CDMA/MT-CDMA channels. In *Proceedings of the 2002 IEEE Military Communications Conference*, Anaheim, CA, vol. 2, pp. 814–819.

[40] J. Namgoong, T. F. Wong, and J. S. Lehnert. 2002. Subspace multiuser detection for multicarrier DS-CDMA. *IEEE Trans. Commun.* 48:1892–908.

[41] M. Peng, Y. J. Guo, and S. K. Barton. 2001. Multiuser detection of asynchronous CDMA with frequency offset. *IEEE Trans. Commun.* 49:952–60.

[42] S. Affes, H. Hansen, and P. Mermelstein. 2002. Interference subspace rejection: A framework for multiuser detection in wideband CDMA. *IEEE J. Selected Areas Commun.* 20:287–302.

[43] B. Smida, S. Affes, J. Li, and P. Mermelstein. 2007. A spectrum-efficient multicarrier CDMA array-receiver with diversity-based enhanced time and frequency synchronization. *IEEE Trans. Wireless Commun.* 6:2315–27.

[44] S. Jomphe, K. Cheikhrouhou, J. Belzile, S. Affes, and J.-C. Thibault. 2005. Area-efficient advanced multiuser WCDMA receiver. In *IEEE Northeast Workshop on Circuits and Systems NEWCAS'05*, pp. 296–99.

[45] H. Hansen, S. Affes, and P. Mermelstein. 2005. *Mathematical derivation of interference subspace rejection*. Technical Report INRS-EMT, EMT-014-0105.

[46] B. Smida and S. Affes. 2005. On the performance of interference subspace rejection for next generation multicarrier CDMA. In *IEEE ISSPA'2005*.

[47] T. S. Rappaport. 1999. *Wireless commmunications: Principles and practice*. Upper Saddle River, NJ: Prentice Hall PTR, pp. 417–435.

[48] B. Smida, S. Affes, and P. Mermelstein. 2003. Joint time-delay and frequency offset synchronization for CDMA array-receivers. In *IEEE SPAWC 2003*, pp. 499–504.

[49] 3rd Generation Partnership Project (3GPP). 2002. *Technical specification group (TSG), radio access network (RAN), UE radio transmission and reception (FDD)*. 3GPP TS 25.101 V5.4.0.

[50] B. Smida, S. Affes, K. Jamaoui, and P. Mermelstein. 2005. A multicarrier-CDMA receiver with full interference suppression and carrier frequency offset recovery. In *IEEE SPAWC'05*, pp. 435–439.

[51] A. Abrardo and D. Sennati. 2000. On the analytical evaluation of closed-loop power-control error statistics in DS-CDMA cellular systems. *IEEE Trans. Veh. Technol.* 49:2071–80.

[52] Y. Lie-Liang and L. Hanzo. 2003. Performance of generalized multicarrier DS-CDMA using various chip waveforms. *IEEE Trans. Commun*. 51:748–52.

[53] Q. M. Rahman and A. B. Sesay. 2001. Performance analysis of MT-CDMA system with diversity combining. *In IEEE MILCOM 2001*, vol. 2, pp. 1360–1364.

[54] S. Kondo and B. Milstein. 1996. Performance of multicarrier DS CDMA systems. *IEEE Trans. Commun*. 44:238–246.